J. Fluid Mech. (2023), *vol*. 973, A46, doi:10.1017/jfm.2023.779

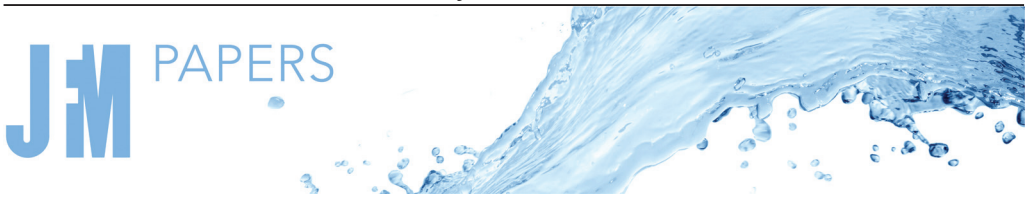

The role of soluble surfactant in the linear instability of a film coating inside a tube

Sheng Li[1], **Ya-Zhou Chen**[1], **Ze Cheng**[1] **and Jie Peng**[1],†

[1]Department of Engineering Mechanics, Tsinghua University, Beijing 100084, PR China

(Received 13 March 2023; revised 8 September 2023; accepted 11 September 2023)

This study investigates the linear instability of a thin-film coating inside a rigid tube. The flow is assumed to be inertialess and driven by an axial body force (e.g. gravity), an interfacial shearing force, or their combinations. The interface and the bulk of the film are laden with soluble surfactant. The properties of the soluble surfactant, i.e. solubility, sorption kinetics and bulk diffusivity, modulate the interfacial dynamics of the film. The influence of these properties on the linear instability of the film is comprehensively investigated via long-wave approximation analysis and numerical calculation. Two modes, namely the interface mode and the surfactant mode, are identified to dominate the instability. For a quiescent film, it is found that solubility, sorption kinetics and bulk diffusivity act to improve the uniformity of the surface surfactant and mitigate the stabilizing effect of the Marangoni force. For the film driven by the axial body/interfacial shearing force, the results reveal that solubility plays contrasting roles in the interface mode and the surfactant mode. A window with intermediate solubility is detected where the film can be linearly stabilized. Moreover, sorption kinetics is found to destabilize the perturbations with long wavelength whereas it stabilizes the perturbations with finite wavelength. The bulk diffusivity of the surfactant has a non-monotonic influence on the flow instability, and the film can be relatively stable at both strong and weak diffusivity.

Key words: thin films, Marangoni convection

1. Introduction

A film coating inside a tube has received long-standing attention from various concerns of scientific investigation. For engineering processes, water-lubricated transport of oil (Joseph *et al.* 1997), film condensation for heat exchange (Dalkilic & Wongwises 2009) and lab-on-a-chip microfluidics (Stone, Stroock & Ajdari 2004) are typical applications of this phenomenon. In pathological investigations, the film flow is also of great significance. Surface tension may drive the film inside the pulmonary airways to form plugs and lead

† Email address for correspondence: peng-jie@tsinghua.edu.cn

to the closure of the airway (Grotberg 2001), which is the typical symptom of respiratory distress syndrome.

Such flow is susceptible to Rayleigh–Plateau instability. Rayleigh (1892) demonstrated that when the wavelength of an initial perturbation exceeds the circumference of the core, surface tension will break the core into pockets. Goren (1962) first investigated the linear instability of such films in the absence of base flow. It was found that the Rayleigh–Plateau instability can initiate a mode with the largest growth rate and lead to the formation of plugs. Hammond (1983) studied the instability of such films via lubrication theory. A nonlinear equation for the evolution of the interface was derived, and it was found that small axisymmetric perturbations with sufficiently long wavelength could destabilize the film. Similar results can also be observed when the film is subject to gravity. Hasegawa & Nakaya (1970) and Krantz & Zollars (1976) solved the Orr–Sommerfeld equation of the problem separately. Their results demonstrated that compared with the planar case, the instability of the film coating inside a tube is intensified by capillary force arising from circumferential curvature. Camassa, Ogrosky & Olander (2014) formulated long-wave asymptotic models for the problem and proposed that absolute instability can be a criterion for plug formation. Camassa, Ogrosky & Olander (2017) later considered the effect of the core flow by a local Poiseuille approach.

A common practice in most applications is to use surfactant to alleviate the surface tension and modulate the dynamics of the interface. The inhomogeneous distribution of surfactant will give rise to a gradient of the surface tension, i.e. the Marangoni force, along the interface. For a quiescent film contaminated with insoluble surfactant, plug formation in both compliant and rigid airways was studied by Halpern & Grotberg (1993) and Otis *et al.* (1993), respectively. They showed that the Marangoni force pulls fluid into the regions where the film is thin. This retards closure of the airway and enhances the stability of the film. Kwak & Pozrikidis (2001) reached the same conclusion by conducting an investigation of the instability of a liquid thread and an annular layer. Two modes of the problem are identified: one is permanently stable and the other is unstable when the wavelength of the perturbation exceeds the circumference of the unperturbed interface.

However, the situation becomes intricate in the presence of base flow. The surfactant will be redistributed due to the advection of the base flow, which may reshape the influence of the Marangoni force. This, in turn, affects the base flow itself and brings complex dynamics to the film. Frenkel & Halpern (2002) and Halpern & Frenkel (2003) reported that insoluble surfactant can trigger the non-inertial instability of a two-layer shear flow, even if it is stable in the quiescent case. This is attributed to the fact that the base flow shifts the phase between the perturbation of the surfactant and the interfacial deflection to make them out of phase. This induces the Marangoni force to drive the flow from the interfacial trough to the interfacial crest and destabilizes the film. This instability was later confirmed by Blyth & Pozrikidis (2004) using a lubrication model. They also investigated the nonlinear saturation of the instability and the nonlinear dynamics of the wave. A similar case in core–annular flow was investigated by Wei & Rumschitzki (2005) and Wei (2005). They found that the base flow accumulates insoluble surfactant at the place where the annulus is thin. They also reported the non-monotonic influence of the Marangoni number, which is expected to induce maximum instability at an intermediate magnitude. Via a normal-mode linear instability analysis, Blyth, Luo & Pozrikidis (2006) identified the dominant modes of the problem, i.e. the interface mode and the surfactant mode, in the context of Stokes flow. They found that the interface mode is responsible for the flow instability. Zhou *et al.* (2014) studied the linear instability of core–annular and viscoelastic film with insoluble surfactant. The film is subject to an axial body force (e.g.

gravity), and the effect of the air core is simplified to a constant shear. Their results showed that various base flows by arbitrary combinations of gravity and shear can induce complex dynamics, including stabilization, destabilization at long wavelength and destabilization at finite wavelength. Recently, based on the model of Camassa *et al.* (2017), Ogrosky (2021) investigated in depth a similar formulation in the background of pulmonary flow.

Generally, surfactant is more or less soluble. Solubility, sorption kinetics and bulk diffusivity of surfactant are also important factors influencing surfactant dynamics. Adsorption/desorption of surfactant at the interface can modulate the Marangoni force and thereby influence flow instability. It was commonly believed that mass exchange between the surface surfactant and the bulk surfactant can alleviate the interfacial gradient of the surfactant. The investigation of a film down an inclined plane (Karapetsas & Bontozoglou 2013, 2014) well supports the idea. The presence of solubility has been found to attenuate the stabilizing effect of the Marangoni force, thereby aggravating the instability of the film. This is due to the fact that the surfactant flux from the bulk to the interface is nearly 90° out of phase with interfacial deflection; this helps the advection of surfactant perturbation by the base flow to counter the advective transport by flow perturbation and thus reduces the interfacial gradient of the surfactant. D'Alessio *et al.* (2020) considered both the solutocapillary effect of soluble surfactant and the thermocapillary effect, and reached the same conclusion. Kalogirou & Blyth (2019, 2020, 2021) investigated a two-layer shear flow with soluble surfactant dissolving in the lower layer. They reported that solubility and sorption kinetics could influence interfacial dynamics and the effect of soluble surfactant on the instability could be either stabilizing or destabilizing. They also noticed that mass exchange of surfactant could strengthen the perturbation of surface surfactant in a certain range of solubility or viscosity ratio.

The presence of soluble surfactant is not rare in investigations involving core–annular flow. Campana & Saita (2006) studied plug formation in airways and found the closure time decreased with an increase of surfactant solubility. Their results indicate that the ability of a surfactant to suppress the Rayleigh instability is diminished by solubility. Muradoglu *et al.* (2019) investigated the propagation and rupture of a liquid plug with soluble surfactant. They found that it is necessary to consider surfactant solubility in core–annular flow, for soluble surfactant can avoid excessive accumulation of the surfactant at the interface and lead to a better estimation of mechanical stress and rupture time. Romanò, Muradoglu & Grotberg (2022) investigated the role of soluble surfactant in a nonlinear airway closure model. Regarding the parameters they adopted, they found that the parameters relating to solubility had little effect on airway closure. Craster, Matar & Papageorgiou (2009) studied a jet laden with soluble surfactant. They found that solubility will weaken the Marangoni force, accelerate the breakup of the jet and lead to the formation of large drops. While previous investigations mainly focused on the nonlinear dynamics of the flow, a fundamental understanding of the effect of soluble surfactant has not been well established. This motivates our investigation of the linear instability of a film with soluble surfactant coating inside a tube. Our investigation encompasses the influence of surfactant solubility, sorption kinetics and bulk diffusivity of the soluble surfactant. We discuss a quiescent film and a flowing film driven by an axial body force and an interfacial shearing force. The mechanism of how soluble surfactant influences interfacial dynamics is discussed.

In this study, the linear instability analysis is carried out under the temporal framework, which is generally adopted in previous literature (Camassa *et al.* 2014; Ogrosky 2021; Jain, Sharma & Das 2022). It provides valuable insights into the long-time behaviour of film flow and helps us understand the impact of soluble surfactant on linear instability.

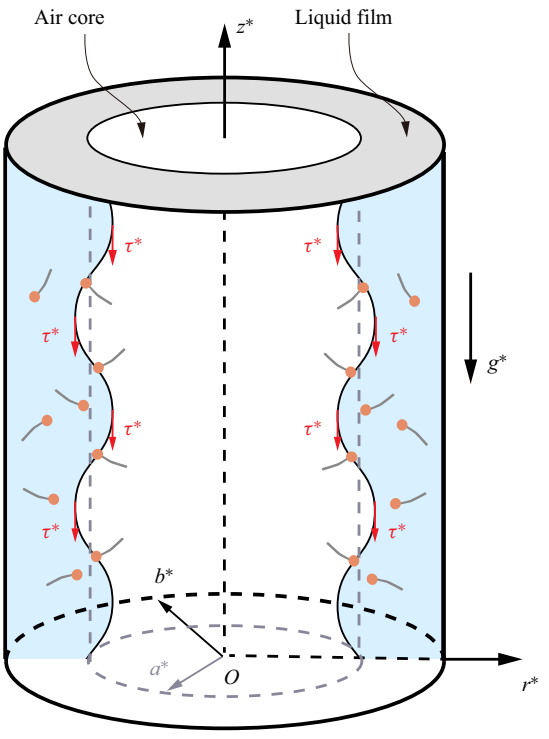

Figure 1. The geometry of a liquid film with soluble surfactant flowing down a tube with an interfacial shearing stress. The grey dashed lines denote the radius of the unperturbed interface.

By solving a linear eigenvalue problem, we can easily determine the temporal growth rates of the perturbations, which can serve as a foundation for conducting in-depth analysis of the instability of the film flow. Since the growth rates of the perturbation for the film flow are small (Brevdo *et al.* 1999), the spatial instability can also be revealed through Gaster transformation (Gaster 1962) or Taylor expansion (Xu *et al.* 2023). The remaining content of this paper is arranged as follows. In § 2, the physical description and mathematical formulation of the problem are introduced. The linearized model is derived by a normal-mode analysis. In § 3, a long-wave approximation analysis is performed and the most dangerous modes, the interface mode and the surfactant mode, are investigated. In § 4, numerical results for the perturbations with finite wavelength are presented. Finally, conclusions are given in § 5.

2. Problem formulation

We investigate a film coating inside a rigid tube in the presence of soluble surfactant, as depicted in figure 1. It occupies an annular region between an air core with $r^* = a^*$ and a rigid tube wall with $r^* = b^*$. The liquid–air interface is initially flat and evolves spatially and temporally with its radius denoted by $\eta^*(z^*, t^*)$. The film is considered to be incompressible and Newtonian, with constant density ρ^* and viscosity μ^*. It is driven by an axial body force g^* and an interfacial shearing stress τ^* exerted by the airflow. The surfactant is assumed to reside both at the liquid–air interface and in the liquid bulk with different diffusivities $\mathcal{D}_s^*$ and $\mathcal{D}_b^*$, which are referred to as surface surfactant and bulk surfactant. Corresponding concentrations of the surface surfactant and the bulk surfactant

are denoted by $\Gamma^*(z^*, t^*)$ and $C^*(r^*z^*, t^*)$, respectively. The surfactant can be adsorbed by or desorbed from the liquid–air interface with adsorption kinetic rate k_a^* or desorption kinetic rate k_d^*.

For the sake of brevity, we present the model in dimensionless form directly by using the following scales:

$$\left.\begin{aligned} t = \frac{t^*}{b^*/U_0^*}, \quad \{r, z\} = \frac{1}{b^*}\left\{r^*, z^*\right\}, \quad \{u, \omega\} = \frac{1}{U_0^*}\left\{u^*, \omega^*\right\}, \\ \{p, \tau\} = \frac{1}{\gamma_0^*/b^*}\left\{p^*, \tau^*\right\}, \quad \Gamma = \Gamma^*/\Gamma_\infty^*, \quad C = C^*/C_{CMC}^*. \end{aligned}\right\} \tag{2.1}$$

Here, γ_0^* is the surface tension of the clean interface, b^* and γ_0^*/b^* are the characteristic length and pressure/stress, respectively, $U_0^* = \gamma_0^*/\mu^*$ is the characteristic velocity, Γ_∞^* denotes the maximum packing concentration of the surfactant at the liquid–air interface and C_{CMC}^* is the critical micelle concentration of the bulk surfactant, above which the bulk surfactant will aggregate into micelles.

2.1. *Governing equations and base flow*

The film flow is governed by the continuity equation and Navier–Stokes equations:

$$\frac{1}{r}\frac{\partial\,(ru)}{\partial r} + \frac{\partial \omega}{\partial z} = 0, \tag{2.2a}$$

$$Re\left(\frac{\partial u}{\partial t} + u\frac{\partial u}{\partial r} + \omega\frac{\partial u}{\partial z}\right) = -\frac{\partial p}{\partial r} + \left[\frac{1}{r}\frac{\partial}{\partial r}\left(\frac{r\partial u}{\partial r}\right) + \frac{\partial^2 u}{\partial z^2} - \frac{u}{r^2}\right], \tag{2.2b}$$

$$Re\left(\frac{\partial \omega}{\partial t} + u\frac{\partial \omega}{\partial r} + \omega\frac{\partial \omega}{\partial z}\right) = -\frac{\partial p}{\partial z} + \left[\frac{1}{r}\frac{\partial}{\partial r}\left(\frac{r\partial \omega}{\partial r}\right) + \frac{\partial^2 \omega}{\partial z^2}\right] - Bo. \tag{2.2c}$$

Here, u represents the radial velocity, ω denotes the axial velocity, $Re = \rho^* b^* U_0^*/\mu^*$ is the Reynolds number and $Bo = \rho^* g^*\, b^{*\,2}/\gamma_0^*$ is the Bond number, which measures gravity or any other axial body force alike. A film with axisymmetric flow is considered since the axisymmetric perturbations give rise to the most dangerous modes for both clean (Hu & Patankar 1995) and contaminated (Blyth & Bassom 2013) liquid–air interfaces.

The boundary conditions at the liquid–air interface $r = \eta(z, t)$, including the kinematic condition, the balance of the normal and tangential stresses, can be expressed as

$$u = \frac{\partial \eta}{\partial t} + \omega\frac{\partial \eta}{\partial z}, \tag{2.3a}$$

$$\sigma_{rr} - 2\frac{\partial \eta}{\partial z}\sigma_{rz} + \left(\frac{\partial \eta}{\partial z}\right)^2 \sigma_{zz} = \Delta_\eta^2\left[(p - p_{in}) + 2\gamma\kappa\right], \tag{2.3b}$$

$$\frac{\partial \eta}{\partial z}\left(\sigma_{rr} - \sigma_{zz}\right) + \left(2 - \Delta_\eta^2\right)\sigma_{rz} = -\Delta_\eta^2\tau - \Delta_\eta\frac{\partial \gamma}{\partial z}, \tag{2.3c}$$

where κ is the mean curvature:

$$\kappa = \frac{1}{2}\left(\frac{1}{\eta\Delta_\eta} - \frac{1}{\Delta_\eta^3}\frac{\partial^2 \eta}{\partial z^2}\right), \tag{2.4}$$

with $\Delta_\eta = \sqrt{1+\eta_z^2}$. Parameter γ is the surface tension, which depends on the concentration of the surface surfactant and can be expressed as

$$\gamma = 1 + Ma \ln(1-\Gamma). \tag{2.5}$$

Here, $Ma = RT^*\Gamma_\infty^*/\gamma_0^*$ is the Marangoni number. Parameter p_{in} denotes the pressure of the air core and τ measures the mean interfacial shearing force exerted by the air flow. In this study, we mainly try to uncover the effect of soluble surfactant on the liquid film instability in the presence of base flow. For simplification, the flow of the liquid film and the air core are fully decoupled. The influence of the air core on the film dynamics is included by considering the pressure outside the liquid film and the interfacial shearing stress. The effect of the liquid film flow on the dynamics of the air core is ignored since the liquid thickness is small. Therefore, both the pressure p_{in} and the shearing stress τ on the liquid–air interface are assumed to be constant, which can be treated as a low-order approximation. Similar treatment can also be found in previous literature (Wei 2005; Samanta 2014; Zhou *et al.* 2014). The expressions of $(\sigma_{rr}, \sigma_{rz}, \sigma_{zz})$ are

$$\sigma_{rr} = 2\frac{\partial u}{\partial r}, \quad \sigma_{rz} = \frac{\partial w}{\partial r} + \frac{\partial u}{\partial z}, \quad \sigma_{zz} = 2\frac{\partial w}{\partial z}. \tag{2.6a–c}$$

At the tube wall $r = 1$, the no-slip condition is imposed:

$$u(1) = 0, \quad \omega(1) = 0. \tag{2.7a–b}$$

The advection–diffusion equation of the surfactant in the bulk can be expressed as

$$\frac{\partial C}{\partial t} + u\frac{\partial C}{\partial r} + \omega\frac{\partial C}{\partial z} = \frac{1}{Pe_b}\left(\frac{1}{r}\frac{\partial}{\partial r}\frac{r\partial C}{\partial r} + \frac{\partial^2 C}{\partial z^2}\right). \tag{2.8}$$

Here, $Pe_b = U_0^* b^*/\mathcal{D}_b^*$ is the Péclect number of the bulk surfactant. It signifies the relative importance of the molecular diffusivity of the bulk surfactant compared with the advective transport. The transport equation of the surface surfactant is derived based on the corresponding expression for insoluble surfactant (Peng & Zhu 2010; Zhou *et al.* 2014; Ogrosky 2021), which reads

$$\frac{\partial}{\partial t}\left(\eta\Delta_\eta\Gamma\right) + \frac{\partial}{\partial z}\left(\omega\eta\Delta_\eta\Gamma\right) = \frac{1}{Pe_s}\frac{\partial}{\partial z}\left(\frac{\eta}{\Delta_\eta}\frac{\partial\Gamma}{\partial z}\right) + \eta\Delta_\eta J_b. \tag{2.9}$$

Here, $Pe_s = U_0^* b^*/\mathcal{D}_s^*$ is the Péclect number of the surface surfactant. It should be noted that (2.9) is essentially equivalent to that proposed by Stone (1990) and Wong, Rumschitzki & Maldarelli (1996). The mass exchange of the surfactant between the bulk and the interface is described by a source J_b, which indicates the surfactant flux from the bulk to the interface. It can be given according to the Langmuir isotherm (Edwards, Brenner & Wasan 1991):

$$J_b = Bi\left[K_b C(1-\Gamma) - \Gamma\right]. \tag{2.10}$$

Here, $Bi = b^* k_d^*/U_0^*$ is the Biot number, which is the ratio between the characteristic time scale of the film flow b^*/U_0^* and the time scale for desorption $(k_d^*)^{-1}$ (Booty & Siegel 2010). It measures the sorption kinetics of the surfactant. When $Bi \ll 1$, desorption of the surface surfactant from the liquid–air interface is suppressed. This tends to reduce the problem to the situation with insoluble surfactant. Parameter $K_b = k_a^* C_{CMC}^*/k_d^*\Gamma_\infty^*$ is the ratio between the adsorption and desorption strength of the surfactant, which denotes the

surfactant's affinity to the interface (Craster *et al.* 2009). It is clear that the solubility of the surfactant becomes weak as K_b increases. Following Fick's law, the boundary condition of the bulk surfactant at the liquid–air interface is

$$\frac{\partial C}{\partial r} - \frac{\partial \eta}{\partial z}\frac{\partial C}{\partial z} = \Delta_\eta Pe_b \beta J_b. \tag{2.11}$$

Here, $\beta = \Gamma^*_\infty / b^* C^*_{CMC}$ indicates the ratio between the surfactant capacity of the film interface and that of the bulk. As β increases, more surfactant is located on the film interface. As a result, it is equivalent to weakening the solubility of the surfactant. It is worth noting that K_b and β exhibit almost the same influence on the solubility. The product $R_b = \beta K_b$ is more indicative to describe the surfactant solubility (Karapetsas & Bontozoglou 2013; Kalogirou & Blyth 2019). The surfactant is highly soluble with $R_b \ll 1$, whereas it is sparingly soluble with $R_b \gg 1$. At the tube wall $r = 1$, it is assumed that no bulk surfactant is absorbed. The corresponding boundary condition can be expressed as

$$\frac{\partial C}{\partial r} = 0. \tag{2.12}$$

In this study, we are concerned with the linear instability of a liquid film driven by an axial body force and an interfacial shearing stress, which is assumed to be of annular geometry with $\bar{\eta} = a$. Corresponding solution of the base flow is

$$\bar{u}(r) = 0, \quad \bar{\omega}(r) = \frac{Bo}{4}(1 - r^2 + 2a^2 \ln r) - a\tau \ln r, \quad \bar{p} = p_{in} - \frac{\bar{\gamma}}{a}, \tag{2.13a–c}$$

where an overbar is used to denote the base flow. Here $\bar{\gamma}$ is given by $1 + Ma \ln(1 - \bar{\Gamma})$, where $\bar{\Gamma}$ is the uniform concentration of the surface surfactant for the base flow, which is called uniform base level concentration. At this moment, the surface surfactant $\bar{\Gamma}$ and the bulk surfactant $\bar{C}$ are in equilibrium with $\bar{J}_b = 0$, and (2.10) yields the following relation:

$$\bar{C} = \frac{\bar{\Gamma}}{K_b\left(1 - \bar{\Gamma}\right)}. \tag{2.14}$$

It should be pointed out that when $\bar{C} > 1$, the bulk surfactant will form micelles. However, in this study, we only consider the situation where $\bar{C} < 1$, which allows us to focus on the specific properties of the soluble surfactant, i.e. solubility, sorption kinetics and bulk diffusivity.

2.2. *Formulation of the linear instability problem*

A standard normal-mode method is adopted to investigate the linear instability of the system. An infinitesimal perturbation $(\hat{\eta}, \hat{u}, \hat{w}, \hat{p}, \hat{\Gamma}, \hat{C})$ is applied to the base flow. Accordingly, we assume that

$$\begin{aligned}&\{\eta(z,t), u(r,z,t), \omega(r,z,t), p(r,z,t), \Gamma(z,t), C(r,z,t)\}\\ &\quad = \left\{a, 0, \bar{\omega}(r), \bar{p}, \bar{\Gamma}, \bar{C}\right\} + \left\{\hat{\eta}, \hat{u}(r), \hat{\omega}(r), \hat{p}(r), \hat{\Gamma}, \hat{C}(r)\right\} \exp(\mathrm{i}k(z - ct)) + \text{c.c.},\end{aligned} \tag{2.15}$$

where k is the real wavenumber and c is the complex wave celerity. Corresponding linearized governing equations of the film flow and the bulk surfactant yield

$$\mathrm{D}\hat{u}\,(r) + \frac{\hat{u}\,(r)}{r} + \mathrm{i}k\hat{\omega}\,(r) = 0, \tag{2.16a}$$

$$\left(\nabla^2 - k^2 - r^{-2}\right)\hat{u}\,(r) = \mathrm{D}\hat{p}\,(r)\,, \tag{2.16b}$$

$$\left(\nabla^2 - k^2\right)\hat{\omega}\,(r) = \mathrm{i}k\hat{p}\,(r)\,, \tag{2.16c}$$

$$\left(\nabla^2 - k^2\right)\hat{C}\,(r) = \mathrm{i}kPe_b\,(\bar{\omega} - c)\,\hat{C}\,(r)\,, \tag{2.16d}$$

where $\mathrm{D} = \mathrm{d}/\mathrm{d}r$ and $\nabla^2 = \mathrm{D}^2 + \mathrm{D}/r$. Here, the fluid inertia is ignored by setting $Re = 0$, which is feasible for film flow with a relatively small velocity. Linearizing the boundary conditions at the liquid–air interface $r = a$, we obtain

$$\hat{u} = \mathrm{i}k\,(\bar{\omega} - c)\,\hat{\eta}, \tag{2.17a}$$

$$\hat{p} - \bar{\gamma}\left(a^{-2} - k^2\right)\hat{\eta} + 2\left(\mathrm{i}k\mathrm{D}\bar{\omega}\hat{\eta} - \mathrm{D}\hat{u}\right) = \frac{Ma}{a\left(1 - \bar{\Gamma}\right)}\hat{\Gamma}, \tag{2.17b}$$

$$\mathrm{i}k\hat{u} + \mathrm{D}\hat{\omega} + \mathrm{D}^2\bar{\omega}\hat{\eta} = \mathrm{i}k\frac{Ma}{1 - \bar{\Gamma}}\hat{\Gamma}, \tag{2.17c}$$

$$\mathrm{D}\hat{C}\,(a) = Pe_b\beta_b\hat{J}_b, \tag{2.17d}$$

$$\hat{J}_b = BiK_b\left(1 - \bar{\Gamma}\right)\hat{C} - Bi\left(K_b\bar{C} + 1\right)\hat{\Gamma}. \tag{2.17e}$$

The linearized form of the surface surfactant transport equation (2.9) can be written as

$$-\mathrm{i}kc\hat{\Gamma} = \hat{J}_b + SF^{(dif)} - SF^{(adv)} - SF^{(per)}. \tag{2.18}$$

Here, $SF^{(dif)} = -k^2/Pe_s\hat{\Gamma}$ is produced by the diffusion of the surface surfactant, $SF^{(adv)} = \mathrm{i}k\bar{\omega}(a)\hat{\Gamma}$ represents the transport of the surface surfactant perturbation due to the base flow and $SF^{(per)} = \bar{\Gamma}\hat{u}(a)/a + \mathrm{i}k\bar{\Gamma}[\hat{\omega}(a) + \mathrm{D}\bar{\omega}(a)\hat{\eta}]$ stands for advective transport of the surface surfactant by the perturbed flow. Combined with (2.15), it is clear that as $\mathrm{Re}(\hat{J}_b\exp(\mathrm{i}k(z - ct))) > 0$, the surfactant is absorbed from the bulk to the interface and the concentration of the surface surfactant is increased; the opposite holds when $\mathrm{Re}(\hat{J}_b\exp(\mathrm{i}k(z - ct))) < 0$. Furthermore, according to (2.18), it is obvious that $\mathrm{Re}(SF^{(dif)}\exp(\mathrm{i}k(z - ct))) > 0$ corresponds to the accumulation of the surface surfactant whereas $\mathrm{Re}(SF^{(dif)}\exp(\mathrm{i}k(z - ct))) < 0$ corresponds to the depletion of the surface surfactant. Similarly, for $SF^{(adv)}\exp(\mathrm{i}k(z - ct))$ and $SF^{(per)}\exp(\mathrm{i}k(z - ct))$, when the real parts of these two terms are positive, they tend to produce net efflux of the surface surfactant and decrease the concentration of the surface surfactant. When they are negative, the effects are reversed.

The boundary condition at the tube wall $r = 1$ can be linearized as

$$\hat{u}\,(1) = 0, \quad \hat{\omega}\,(1) = 0, \quad \mathrm{D}\hat{C}\,(1) = 0. \tag{2.19a–c}$$

It is worth noting that the relationship between c and $(\hat{\eta}, \hat{\Gamma}, \hat{C})$ can be determined explicitly according to (2.16*d*), (2.17*a*) and (2.18). In the following, the analysis will hinge on dynamics described by these equations.

3. The long-wave approximation analysis

In this section, we study the instability of the system in the long-wave limit, i.e. $k \to 0$. The perturbation quantities can be expanded as

$$\begin{aligned}\left\{\hat{\eta}, c, \hat{u}(r), \hat{\omega}(r), \hat{p}(r), \hat{\Gamma}, \hat{C}(r)\right\} = &\left\{\hat{\eta}_0, c_0, k\hat{u}_0(r), \hat{\omega}_0(r), \hat{p}_0(r), \hat{\Gamma}_0, \hat{C}_0(r)\right\} \\ &+ k\left\{\hat{\eta}_1, c_1, k\hat{u}_1(r), \hat{\omega}_1(r), \hat{p}_1(r), \hat{\Gamma}_1, \hat{C}_1(r)\right\} \\ &+ O\left(k^2\right). \end{aligned} \tag{3.1}$$

Here, considering the continuity equation (2.16*a*), $\hat{u}$ is one order of magnitude greater than $\hat{\omega}$ and thus expanded from the $O(k)$ scale. Substituting (3.1) into (2.16)–(2.19*a–c*), and equating items with the same order of k separately, we obtain equations of each order. We focus on the perturbation modes of the system, and the role of the surfactant in the instability of these modes. The detailed derivation process is presented in Appendix A.

3.1. *The interface mode and the surfactant mode*

As shown in Appendix A, $(\hat{\eta}_0, \hat{\Gamma}_0, \hat{C}_0)$ satisfy (A8), (A10) and (A15). Similar to Wei (2005), these equations yield two sets of solutions, which correspond to two modes of the problem. One mode is triggered by the deflection of the interface, denoted as the interface mode. The other mode arises from the perturbation of the surface surfactant $\hat{\Gamma}_0$ irrespective of interfacial deflection, which is denoted as the surfactant mode. Apart from these two modes, the transport equation of the bulk surfactant yields infinite modes due to diffusion, which can be derived by expanding c as $k^{-1}c_0 + c_1 + kc_2$ instead, as suggested by Kalogirou & Blyth (2019). However, according to a numerical verification (not presented for brevity), these modes are always stable and are ignored in the following discussion.

For the interface mode, $\hat{\eta}_0$ is set to be unity, and other variables vary proportionally to it. According to (A16*a*), the wave celerity c_0 is independent of surfactant solubility, which is consistent with the insoluble case. Similar phenomena were also observed by Karapetsas & Bontozoglou (2014) and Kalogirou & Blyth (2019). However, according to (A16*b*), $\hat{\Gamma}_0$ is influenced by the advection of the bulk surfactant and surfactant solubility R_b. When $R_b \gg 1$, $\hat{\Gamma}_0$ can be reduced to that of Zhou *et al.* (2014), where the surfactant is assumed to be insoluble. Furthermore, since c_0 is a real number, the instability of the system is determined by the $O(k)$ solution to c_1 with the following expression:

$$c_1 = \mathrm{i}\frac{A_3}{16a^3}\bar{\gamma} + \mathrm{i}\frac{A_4 Ma}{16a^2\left(1-\bar{\Gamma}\right)}\hat{\Gamma}_0. \tag{3.2}$$

Here, A_3 and A_4 are related to the geometrical parameters, as presented in (A1), which are positive definite over $0 < a < 1$. Clearly, for (3.2), the first term on the right-hand side is attributed to the circumferential surface tension, and the second term arises from the Marangoni force. Since $\hat{\Gamma}_0$ is independent of sorption kinetics Bi and bulk surfactant diffusivity Pe_b as shown in (A16*b*), it can be concluded that soluble surfactant can affect the interface mode exclusively through solubility R_b.

For the surfactant mode, we adopt a method similar to that for the interface mode and set $\hat{\Gamma}_0 = 1$ and $\hat{\eta}_0 = 0$. The wave celerity c_0 of the surfactant mode, which is real, is mediated by the transport of the bulk surfactant, as shown in (A23*a*). When the surfactant

is sparingly soluble ($R_b \gg 1$), the perturbation wave travels with interfacial speed $\bar{\omega}(a)$ (Zhou *et al.* 2014); when the surfactant is highly soluble ($R_b \ll 1$), c_0 degenerates into the average speed of the base flow $2\bar{q}/(1-a^2)$ with $\bar{q} = \int_a^1 r\bar{\omega}(r)\,\mathrm{d}r$. The instability of the surfactant mode is determined by $O(k^2)$ problem and c_1 can be expressed as

$$c_1 = \mathrm{i}\left(1 + \frac{1-a^2}{2aR_b\left(1-\bar{\Gamma}\right)^2}\right)^{-1}\left(-\frac{1}{Pe_s} + f_1^{(Pe_b)} + f_1^{(Bi)} + f_1^{(S)} - SF_2^{(per)}\right). \tag{3.3}$$

In the last bracket on the right-hand side of (3.3), the first two terms are attributed to the diffusion of the surface surfactant and the bulk surfactant. Third and fourth terms $f_1^{(Bi)}$ and $f_1^{(S)}$ denote the contribution of the advection of the bulk surfactant by the base flow, which are expressed in (A33). The fifth term is due to the advective transport of the surface surfactant by the perturbed flow with its expression in (A35). From (3.3), it can be deduced that the instability of the surfactant mode is not only modulated by solubility R_b but also affected by bulk diffusivity Pe_b and sorption kinetics Bi. This is different from that of the interface mode.

Before the elucidation of the two modes, it should be pointed out that there is an exceptional situation, when the film is quiescent, i.e. $Bo = 0$ and $\tau = 0$. In this situation, $\hat{\Gamma}_0$ is determined by $O(k^2)$ transport equation of the surface surfactant due to the lack of advection attributed to the base flow. Solutions to the problem are derived by setting $\hat{\eta}_0 = 1$ in Appendix A.5. The results show that $\hat{\Gamma}_0$ for both modes is in the opposite phase of $\hat{\eta}_0$. According to the expression of c_1 (A37), the interface mode, which corresponds to a weaker $\hat{\Gamma}_0$, is more dangerous for instability. As illustrated in figure 2(*a*), $\mathrm{Im}(c_1)$ of the interface mode increases with a decrease of R_b. This is because the non-uniformity of $\hat{\Gamma}_0$ for the interface mode is suppressed with increasing solubility, which acts to attenuate the stabilizing effect of the Marangoni force. Here, we focus on the influence of bulk diffusivity on the linear instability of the system. Thus, the magnitude of Pe_s is assumed to be larger than that of Pe_b. This indicates that the effect of interfacial diffusion is negligible in comparison to bulk diffusion. A similar assumption can also be found in previous literature (Kalogirou & Blyth 2019, 2021). Term $\mathrm{Im}(c_1)$ of the interface mode also increases with increasing bulk diffusivity, i.e. decreasing Pe_b, as illustrated in figure 2(*b*), where the uniformity of the surfactant is improved as well. As a result, decreasing Pe_b makes the quiescent film more unstable.

3.2. *Instability of the film driven by an axial body force*

In this section, we proceed to consider the instability of the film driven by an axial body force, i.e. $\tau = 0$ and $Bo \neq 0$. According to (3.2), c_1 of the interface mode is modulated by Γ_0, which is derived from (A16*b*) (more details can be found in Appendix A):

$$\hat{\Gamma}_0 = \hat{\Gamma}_0^{(ins)}\left(1 + \frac{A_3 + 2A_6}{4aA_1R_b\left(1-\bar{\Gamma}\right)^2}\right)^{-1}, \tag{3.4}$$

with

$$\hat{\Gamma}_0^{(ins)} = -\frac{A_2\bar{\Gamma}}{aA_1}. \tag{3.5}$$

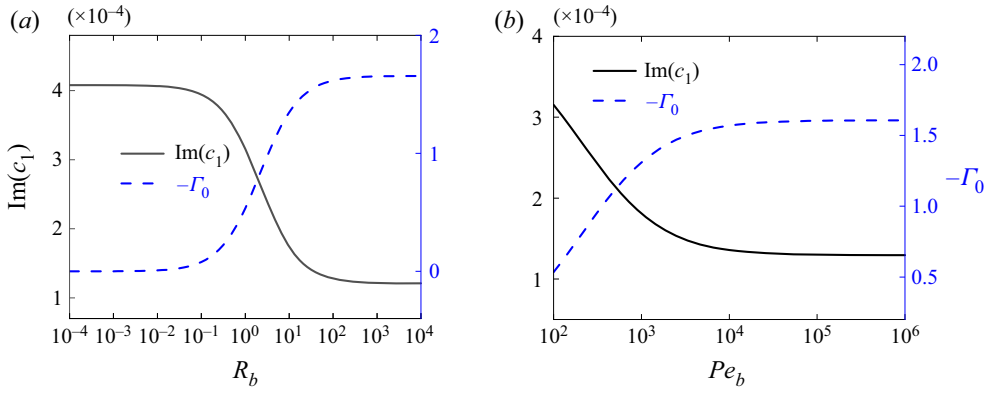

Figure 2. The dependence of $\mathrm{Im}(c_1)$ and perturbed surfactant concentration $\hat{\Gamma}_0$ on (*a*) solubility and (*b*) bulk diffusivity for a quiescent film given by long-wave approximation analysis. In (*a*) $Pe_b = 100$ and in (*b*) $R_b = 1.0$, and the remaining parameters for both cases are: $a = 0.9$, $Re = 0$, $Ma = 0.02$, $\bar{\Gamma} = 0.4$, $Bi = 0.1$ and $Pe_s = 1 \times 10^6$.

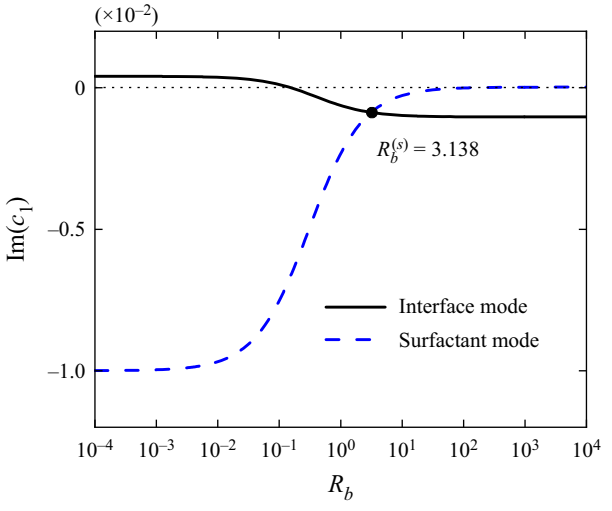

Figure 3. The dependence of $\mathrm{Im}(c_1)$ on solubility R_b for a film driven by an axial body force. The solid line denotes the interface mode and the dashed line denotes the surfactant mode, both given by long-wave approximation analysis. Here $R_b^{(s)}$ is the solubility where the curves of the interface mode and the surfactant mode intersect. The parameters adopted here are $Bo = 1$, $\tau = 0$, $Pe_b = 100$ and the others remain the same as in figure 2.

Here, $\hat{\Gamma}_0^{(ins)}$ is the solution to the corresponding problem with insoluble surfactant. Since $\hat{\eta}_0 = 1$, $\hat{\Gamma}_0$ is in the opposite phase of $\hat{\eta}_0$. This indicates that the concentration of the surface surfactant is higher at the interfacial trough while it is lower at the interfacial crest. The induced Marangoni force directs from the interfacial trough to the crest and the resulting flow acts to stabilize the interface mode. It should be pointed out that the interfacial crest/trough denotes the location with the maximum/minimum radius, which corresponds to the thinnest/thickest location of the film. However, (3.4) suggests that the amplitude of $\hat{\Gamma}_0$ reduces with decreasing R_b. This indicates that solubility plays a destabilizing role in the interface mode, as illustrated in figure 3. This phenomenon

is attributed to the four transport pathways of the surface surfactant defined in (2.18). To better elucidate the problem, a reference frame, which moves with the perturbation wave, is introduced. The transport of the surface surfactant perturbation $SF^{(adv)}$ can be rewritten as $\mathrm{i}k(\bar{\omega}(a) - c_0)\hat{\Gamma}$. Corresponding expressions in the $O(k)$ order can be derived based on (A11):

$$\left.\begin{gathered} SF_1^{(adv)} = -\mathrm{i}\frac{A_1 Bo}{4}\hat{\Gamma}_0, \quad \hat{J}_{b1} = \mathrm{i}\frac{Bo\,(A_3 + 2A_6)}{16aR_b\left(1-\bar{\Gamma}\right)^2}\hat{\Gamma}_0, \\ SF_1^{(per)} = -\mathrm{i}\frac{A_2 Bo}{4a}, \quad SF_1^{(dif)} = 0. \end{gathered}\right\} \tag{3.6}$$

Clearly, the phase of $SF_1^{(adv)}$ lags 90° behind $\hat{\Gamma}_0$, while the phase of adsorption/desorption flux $\hat{J}_{b1}$ precedes $\hat{\Gamma}_0$ by 90°. This means that $SF_1^{(adv)}$ and $\hat{J}_{b1}$ are in anti-phase. According to (2.18), we know that the depletion of the surface surfactant caused by the base flow coincides with the desorption flux from the interface to the bulk. Meanwhile, the accumulation of the surface surfactant caused by the base flow coincides with the adsorption flux from the bulk to the interface. As a result, $\hat{J}_{b1}$ is a boost for $SF_1^{(adv)}$ to counter the surfactant transportation by the perturbed flow $SF_1^{(per)}$, and alleviates the perturbation of the surface surfactant. In this situation, solubility promotes the uniformity of $\hat{\Gamma}_0$. It leads to the attenuation of the stabilizing effect of the Marangoni force and enhances the instability of the interface mode.

For the surfactant mode, the instability is attributed to the accumulation/depletion of the surfactant at the interface. Parameter c_1 of the surfactant mode is expressed in (3.3). Its instability is determined by those five terms in the second bracket on the right-hand side. The first term $-1/Pe_s$ is attributed to the interfacial diffusivity of the surface surfactant, which is weak and generally ignored. Terms $f_1^{(Pe_b)}$, $f_1^{(Bi)}$ and $f_1^{(S)}$ are components of $\hat{J}_{b2}$ (see (A31)) and their magnitude increases with a decrease of R_b. Term $f_1^{(Pe_b)}$ is caused by the diffusion of the bulk surfactant. Recall that the derivation of the surfactant mode is based on $\hat{\Gamma}_0 = 1$. Term $f_1^{(Pe_b)}$ is in the opposite phase to $\hat{\Gamma}_0$ and acts to diminish the perturbation of the surface surfactant. For $f_1^{(Bi)}$, it is obviously non-positive irrespective of Bo and plays a stabilizing role. Furthermore, this conclusion holds even for various combinations of Bo and τ. In $f_1^{(S)}$, the analytical expression of S is too cumbersome to present here. As illustrated in figure 4, the numerical results show that S takes a non-positive value. Thus, it tends to stabilize the surfactant mode. So far, the first four terms in the second bracket on the right-hand side of (3.3) always contribute to stabilizing the surfactant mode. Its instability results from $SF_2^{(per)}$, which denotes the surface surfactant transported by the perturbed flow. Substituting (2.13*a–c*) with $\tau = 0$ into (A35), $SF_2^{(per)}$ can be expressed as

$$SF_2^{(per)} = \frac{A_5 Ma\bar{\Gamma}}{16a^3\left(1-\bar{\Gamma}\right)} - \mathrm{i}\frac{A_2 Bo\bar{\Gamma}}{4a}\hat{\eta}_1, \tag{3.7}$$

which arises from the Marangoni effect and interfacial deflection. According to (A21), $\hat{\eta}_1$ satisfies

$$\hat{\eta}_1 = \hat{\eta}_1^{(ins)}\left(1 + \frac{A_6}{2A_1\left(1 - a^2 + 2aR_b\left(1-\bar{\Gamma}\right)^2\right)}\right)^{-1}, \tag{3.8}$$

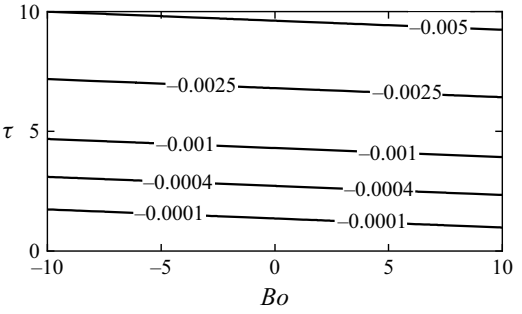

Figure 4. The contour of S on the Bo versus τ plane with $a = 0.9$, $R_b = 1$ and $\bar{\Gamma} = 0.4$.

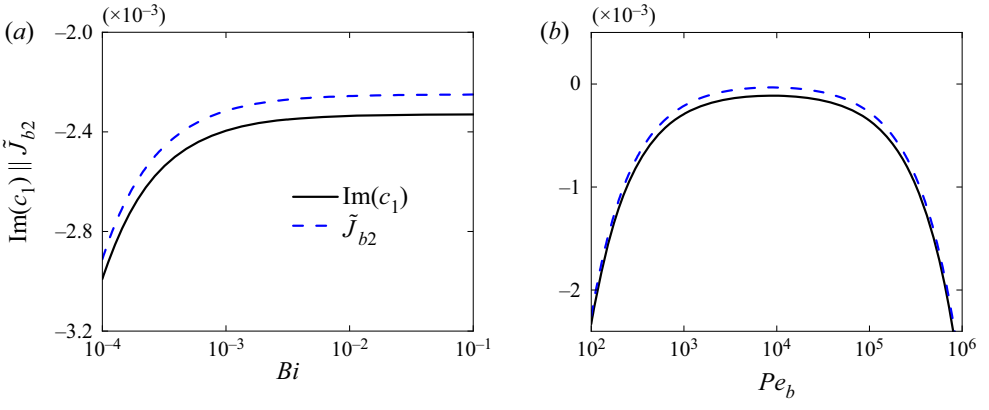

Figure 5. The dependence of $\mathrm{Im}(c_1)$ and perturbed adsorption/desorption flux $\hat{J}_{b2}$ of the surfactant mode on (a) sorption kinetics and (b) bulk diffusivity, where the film is driven by an axial body force. In (a), Pe_b is fixed at 100 and in (b), Bi is fixed at 0.1. For both cases, we take $Bo = 1$, $\tau = 0$, $R_b = 1$ and the other parameters remain the same as in figure 2.

with

$$\hat{\eta}_1^{(ins)} = -\frac{\mathrm{i}A_4 Ma}{4a^2 A_1 Bo\left(1-\bar{\Gamma}\right)}. \tag{3.9}$$

Here, $\hat{\eta}_1^{(ins)}$ is identical to the first-order interfacial deflection in the corresponding problem with insoluble surfactant. According to (3.8) and (3.9), $\hat{\eta}_1$ lags 90° behind $\hat{\Gamma}_0$ and its magnitude is reduced with decreasing R_b. Therefore, the second term on the right-hand side of (3.7) is in the opposite phase to $\hat{\Gamma}_0$. It acts to destabilize the surfactant mode and this destabilizing effect on the surfactant mode diminishes with decreasing R_b. Combining all the terms in (3.3), $\mathrm{Im}(c_1)$ is decreased while R_b decreases as demonstrated in figure 3. Notably, different from the insoluble case (Jain *et al.* 2022), where the surfactant mode is always unstable, the surfactant mode with soluble surfactant could be stable with a certain small R_b.

According to (3.3), we know that the instability of the surfactant mode is modulated by sorption kinetics Bi and bulk diffusivity Pe_b as well. As shown in figure 5(a), the adsorption/desorption flux $\hat{J}_{b2}$ is intensified as Bi decreases, which improves the uniformity of the surface surfactant and stabilizes the surfactant mode. This is attributed to the fact that the effect of $f_1^{(Bi)}$ in (A31) and (A34) is inversely proportional to Bi.

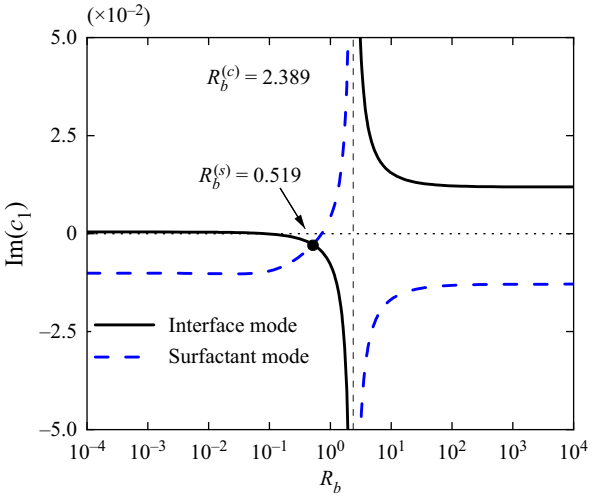

Figure 6. The dependence of Im(c_1) on solubility R_b for a shear-driven film given by long-wave approximation analysis. The solid line denotes the interface mode and the dashed line denotes the surfactant mode. Here $R_b^{(s)}$ is the solubility where the curves of interface mode and surfactant mode intersect. The parameters adopted here are $Bo = 0$, $\tau = 1$, $Pe_b = 100$ and the other parameters are the same as in figure 2. Under current circumstance, the critical solubility $R_b^{(c)} = 2.389$ and is demonstrated as a vertical asymptote.

Moreover, as demonstrated in figure 5(*b*), bulk diffusivity Pe_b has a non-monotonic influence on the instability of the surfactant mode and the surfactant mode is relatively stable for both strong and weak diffusivity. When the bulk diffusivity is strong, i.e. Pe_b is small, $f^{(Pe_b)}$ becomes significant in (A31) and (A34), which leads to strong adsorption/desorption flux and stabilizes the surfactant mode. On the other hand, when Pe_b is sufficiently large, the stabilizing effect of $f_1^{(S)}$ will become significant instead. The reason for this is that the gradient of the bulk surfactant is intensified due to weak diffusion. This results in large adsorption/desorption flux and mitigates the growth rates of the surfactant mode.

3.3. *Instability of the film driven by an interfacial shearing force*

In this section, we examine the instability of film flow driven by an interfacial shearing force, i.e. $Bo = 0$ and $\tau \neq 0$. Figure 6 presents the effect of solubility on the instability for both the interface and the surfactant modes. It is interesting that there is a critical solubility $R_b^{(c)}$, around which Im(c_1) changes dramatically. On both sides of $R_b^{(c)}$, solubility plays a destabilizing role in the interface mode but a stabilizing role in the surfactant mode. Similar to that presented in § 3.2, the effect of the capillary force on the instability of the interface mode is modulated by the surface surfactant perturbation $\hat{\Gamma}_0$, which is determined according to (A11). Each item, which denotes one pathway of the surfactant transport, can be expressed in the reference frame travelling with c as follows:

$$\left.\begin{aligned} SF_1^{(adv)} = \mathrm{i}\frac{A_1\tau}{4}\hat{\Gamma}_0, \quad \hat{J}_{b1} = \mathrm{i}\frac{\tau\,(A_4 - 3A_6)}{16a^2R_b\left(1-\bar{\Gamma}\right)^2}\hat{\Gamma}_0, \\ SF_1^{(per)} = -\mathrm{i}\tau\frac{4a^2 - A_2}{4a^2}, \quad SF_1^{(dif)} = 0. \end{aligned}\right\} \tag{3.10}$$

In this study, the film thickness is assumed to be small ($a = 0.9$). Values of $(A_4 - 3A_6)$ and $(4a^2 - A_2)$ are both positive for a thin liquid film, e.g. $a > 0.53$. Thus, $SF_1^{(adv)}$ and $\hat{J}_{b1}$ are in the same phase, and play a contrasting role in the surface surfactant transport at $O(k)$ order. This is different from that presented in (3.6), and $\hat{\Gamma}_0$, as given by (A16*b*), can be simplified as

$$\hat{\Gamma}_0 = \hat{\Gamma}_0^{(ins)} \frac{R_b}{R_b - R_b^{(c)}}, \tag{3.11}$$

with

$$\hat{\Gamma}_0^{(ins)} = \frac{\bar{\Gamma}(4a^2 - A_2)}{aA_1}. \tag{3.12}$$

Here, $\hat{\Gamma}_0^{(ins)}$ corresponds to the solution of the problem with insoluble surfactant. The critical solubility $R_b^{(c)}$ is

$$R_b^{(c)} = \frac{A_4 - 3A_6}{4aA_1(1 - \bar{\Gamma})^2}. \tag{3.13}$$

Notably, if $SF_1^{(adv)}$ equals $\hat{J}_{b1}$ in (3.10), we have $R_b = R_b^{(c)}$ and infinite $\hat{\Gamma}_0$ according to (3.11). This indicates that the presence of $R_b^{(c)}$ is attributed to the offsetting effect between $SF_1^{(adv)}$ and $\hat{J}_{b1}$ in the surfactant transport. As a result, the surfactant can accumulate/deplete at the interface infinitely due to the presence of $SF_1^{(per)}$. Moreover, when the surfactant is sparingly soluble ($R_b \gg 1$), $\hat{J}_{b1} \to 0$. According to (A11), $SF_1^{(per)}$ is balanced by $SF_1^{(adv)}$. The induced perturbation of surface surfactant is $\hat{\Gamma}_0^{(ins)}$, which is in phase with $\hat{\eta}_0$ and induces destabilizing Marangoni flow from the interfacial crest to the interfacial trough. When R_b reduces, $\hat{J}_{b1}$ becomes large and the surface surfactant transported by $SF_1^{(adv)}$ will be hindered. Consequently, $\hat{\Gamma}_0$ is prone to become concentrated/dilute, which tends to aggravate the instability of the interface mode. However, when R_b is below $R_b^{(c)}$, $\hat{J}_{b1}$ has the advantage over $SF_1^{(adv)}$. According to (A11), we know that $SF_1^{(per)}$ is now mainly balanced by $\hat{J}_{b1}$. Therefore, the phase of $\hat{\Gamma}_0$ is reversed, which induces the Marangoni flow from the trough to the crest and contributes stability to the interface mode. As R_b is further decreased, $\hat{\Gamma}_0$ reduces due to the enhanced adsorption/desorption flux $\hat{J}_{b1}$. The stabilizing effect of the Marangoni flow is then attenuated. It is noted that when R_b approaches $R_b^{(c)}$, $\mathrm{Im}(c_1)$ will tend to be infinite, as shown in figure 6. In fact, under this situation, the current long-wave expansion is inappropriate. Term $\mathrm{Im}(c_1)$ is proportional to $k^{1/2}$ as presented in Appendix B. Similar results for two-layer planar flow have been reported for clean interface (Halpern & Frenkel 2003) and for soluble surfactant (Kalogirou & Blyth 2019). It should be pointed out that the current long-wave expansion only fails in a narrow region of R_b, i.e. $R_b \to R_b^{(c)}$, and it is applicable for the rest of the values of R_b. Halpern & Frenkel (2003) have made an in-depth investigation of this singularity and pointed out that as soon as the parameter moves slightly away from the critical situation, the growth rates rapidly change to the results given by $O(k)$ expansion.

For the surfactant mode, the instability is determined by (3.3) with $Bo = 0$. Similar to film flow driven by an axial body force, the first four terms in the right-hand bracket of

(3.3) play a stabilizing role. Corresponding conclusions in the previous section still hold. Here Bi acts to enhance the instability of the surfactant mode while Pe_b tends to make the surfactant mode relatively stable for both strong (small Pe_b) and weak (large Pe_b) diffusivity. Furthermore, according to (3.3), the instability of the surfactant mode arises from $SF_2^{(per)}$ as well. Substituting (2.13*a–c*) with $Bo = 0$ into (A35), we obtain

$$SF_2^{(per)} = \frac{A_5 Ma\bar{\Gamma}}{16a^3(1-\bar{\Gamma})} - \mathrm{i}\frac{\tau(4a^2 - A_2)\bar{\Gamma}}{4a^2}\hat{\eta}_1, \tag{3.14}$$

where $\hat{\eta}_1$ can be derived via (A25) as

$$\hat{\eta}_1 = \frac{\hat{\eta}_1^{(ins)}}{R_b - R_b^{(c)}}\left(R_b + \frac{1-a^2}{2a(1-\bar{\Gamma})^2}\right). \tag{3.15}$$

Here, $\hat{\eta}_1^{(ins)}$ corresponds to the $O(k)$ order deflection of the liquid–air interface with insoluble surfactant, and its expression is

$$\hat{\eta}_1^{(ins)} = \mathrm{i}\frac{A_4 Ma}{4a\tau A_1(1-\bar{\Gamma})}. \tag{3.16}$$

Comparing (3.7) and (3.14), we observe that the first terms on the right-hand sides of the equations, which play stabilizing roles, are the same. For the second term, the same critical solubility $R_b^{(c)}$ can also be obtained according to (3.15). On both sides of $R_b^{(c)}$, although the second term has opposite phases, it is prone to make the surfactant mode relatively stable with decreasing R_b. As a result, solubility tends to decrease the growth rate of the surfactant mode on both sides of $R_b^{(c)}$ (see figure 6). This is consistent with the role of solubility in film flow driven by an axial body force.

4. The linear instability analysis at finite wavelength

In this section, we investigate the linear instability of the film at finite wavelength, where the high-order perturbation once suppressed in the long-wave regimes will revive due to the increase of wavenumber. This will make an additional contribution to the stability/instability of the film. The influences of surfactant solubility R_b, sorption kinetics Bi and bulk diffusivity Pe_b on the linear instability of the film are mainly concerned. Since a large number of parameters are involved in the problem, it is cumbersome to discuss each one in detail. Therefore, we render results that display representative effects of the soluble surfactant on the linear instability of film flow, with $a = 0.9$, $b = 1.0$, $\bar{\Gamma} = 0.4$, $Re = 0$ and $Pe_s = 1 \times 10^6$.

4.1. *Numerical implementation*

The linearized equations (2.16)–(2.19*a–c*) are discretized by a spectral collocation method based on Chebyshev polynomials (Trefethen 2000). The film region is mapped onto the spectral space $x \in [-1, 1]$ via the following relation:

$$x = 1 - 2\left(\frac{r-a}{1-a}\right), \tag{4.1}$$

where the tube wall and the liquid–air interface are located at $x = -1$ and $x = 1$, respectively. The spectral space is constructed via $N + 1$ Chebyshev points. Governing

(Bo, τ)	Bi	Rb	Long-wave approximation	Numerical results
(1.0, 0.0)	0.1	0.1	$I : 1.17022 \times 10^{-12}$	$I : 1.17022 \times 10^{-12}$
			$S : -7.52810 \times 10^{-11}$	$S : -7.52062 \times 10^{-11}$
(0.0, 1.0)	0.1	1.0	$I : -7.86152 \times 10^{-11}$	$I : -7.86152 \times 10^{-11}$
			$S : 4.13296 \times 10^{-11}$	$S : 4.13479 \times 10^{-11}$
(1.0, 0.1)	0.1	0.1	$I : 4.54293 \times 10^{-13}$	$I : 4.54293 \times 10^{-13}$
			$S : -7.49400 \times 10^{-11}$	$S : -7.48562 \times 10^{-11}$
(1.0, 0.1)	0.1	10.0	$I : -2.43473 \times 10^{-11}$	$I : -2.43473 \times 10^{-11}$
			$S : 1.18338 \times 10^{-11}$	$S : 1.18354 \times 10^{-11}$
(1.0, −0.1)	1.0	1.0	$I : 2.79617 \times 10^{-12}$	$I : 2.79617 \times 10^{-12}$
			$S : -3.23057 \times 10^{-11}$	$S : -3.22926 \times 10^{-11}$

Table 1. Comparison of two dominant growth rates obtained by the long-wave approximation analysis and the numerical method with $k = 1 \times 10^{-4}$. Notation I represents the growth rate for the interface mode and S that for the surfactant mode. The remaining parameters are the same as in figure 2.

equations (2.16) are discretized on this clustering grid, and boundary conditions (2.17)–(2.19*a–c*) are implemented at the boundary points. The perturbation of $\{\hat{u}, \hat{\omega}, \hat{p}, \hat{C}\}$ is expanded on the corresponding Chebyshev polynomials:

$$\left.\begin{aligned} \hat{u}(r) &= \sum_{i=0}^{N} \hat{u}_i T_i(r), \quad \hat{\omega}(r) = \sum_{i=0}^{N} \hat{\omega}_i T_i(r), \\ \hat{p}(r) &= \sum_{i=0}^{N} \hat{p}_i T_i(r), \quad \hat{C}(r) = \sum_{i=0}^{N} \hat{C}_i T_i(r), \end{aligned}\right\} \tag{4.2a–d}$$

where $T_i(r)$ is the ith Chebyshev polynomials of the first kind. The above discretization renders a generalized complex eigenvalue problem $\boldsymbol{AX} = \Omega \boldsymbol{BX}$. Here, $\boldsymbol{X} = \{\hat{u}_i, \hat{\omega}_i, \hat{p}_i, \hat{C}_i, \hat{\eta}, \hat{\Gamma}\}$ is the perturbed variables and consists of $4N + 6$ elements. Matrices $\boldsymbol{A}$ and $\boldsymbol{B}$ are complex matrices, which are determined by dimensionless parameters Bo, τ, R_b, Bi, Pe_b and Pe_s. Eigenvalue $\Omega = \Omega_r + \mathrm{i}\Omega_i$ is the complex eigenvalue, and its imaginary part Ω_i corresponds to the growth rate at a given wavenumber. The built-in QZ algorithm eig of MATLAB is adopted to obtain the complex eigenvalues and eigenvectors. We utilize Advanpix (Advanpix 2022), a multi-precision computing toolbox, to ensure computing precision, which enables MATLAB to run with arbitrary precision and meanwhile with high efficiency. The code is verified by comparing the numerical results with those of the long-wave approximation analysis, as listed in table 1. They are consistent when the perturbation wavenumber is relatively small, e.g. $k = 1 \times 10^{-4}$. Moreover, in figure 7(*a*), the results obtained by Zhou *et al.* (2014) for a liquid film coating inside a tube with insoluble surfactant are reproduced by setting $Bi = 0$ or $R_b \gg 1$. When $a \to 1$, the film coating inside a tube with soluble surfactant can be reduced to a planar falling film. As shown in figure 7(*b*), the results are consistent with those presented by Karapetsas & Bontozoglou (2013).

4.2. *The quiescent film*

Figure 8(*a*) shows the growth rates of the perturbation wave with $Bi = 0.1$, $Pe_b = 100$ and various solubilities R_b. The film is assumed to be quiescent. When the surfactant is

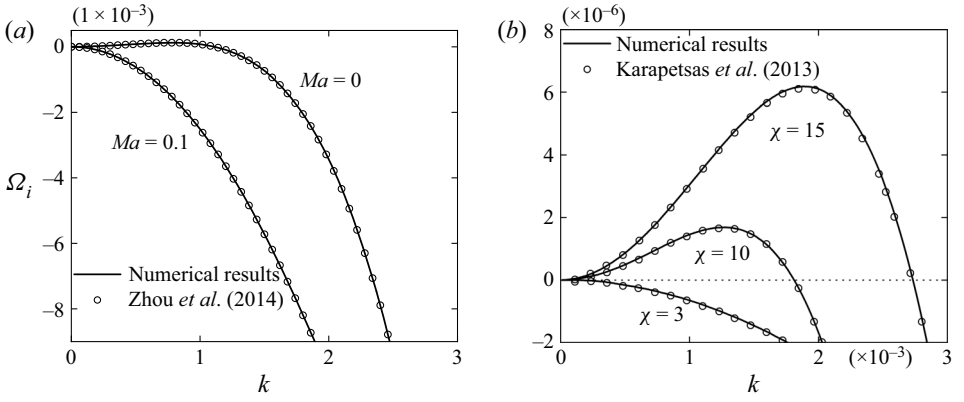

Figure 7. Validation of the numerical method with the results of (*a*) Zhou *et al.* (2014) and (*b*) Karapetsas & Bontozoglou (2013). (*a*) Results of a liquid film coating inside a tube with insoluble surfactant with $a = 0.9$, $Bo = 5$ and $\tau = -0.4$. Our results are obtained by taking the insoluble limit, $R_b \gg 1$ or $Bi = 0$. (*b*) Results for a falling planar film with soluble surfactant. Our results approximate to the situation via letting the film be extremely thin, e.g. $1 - a = 1 \times 10^{-6}$. The parameters used in (*b*) follow the definitions of Karapetsas & Bontozoglou (2013).

sparingly soluble with $R_b = 100$, the growth rates are nearly indistinguishable from those of insoluble surfactant. When R_b is reduced, e.g. from 100 to 0.1, the flow instability is enhanced. This is in line with the prediction of the long-wave approximation analysis. At $R_b = 0.1$, the surfactant is highly soluble and the perturbation of the surface surfactant will be mitigated by the adsorption/desorption flux. Therefore, the film will experience uniform but decreased surface tension. Corresponding growth rates are a little lower than those of the problem with clean interface. The cut-off wavenumber equals the reciprocal of the unperturbed interfacial radius a, the same as for the film with clean interface (Hammond 1983) or insoluble surfactant (Wei & Rumschitzki 2005). Similar results can be observed in figure 8(*b*), where the cut-off wavenumbers remain $1/a$ for various Pe_b. Moreover, the film instability can be strengthened as Pe_b decreases. Figure 8(*c*) compares the growth rates of the perturbation wave with $R_b = 1.0$, $Pe_b = 100$ and various Bi. Similar to previous cases, the cut-off wavenumbers are fixed at $1/a$. It is found that the growth rates increase with increasing Bi. This may be attributed to the fact that the adsorption/desorption flux, which mitigates magnitude of surface surfactant, is strengthened with increasing Bi. As a result, the stabilizing effect of the Marangoni force is attenuated. Readers may notice that sorption kinetic Bi does not involve in the long-wave instability as shown in (A37). This is because the surfactant at the interface and in the bulk is able to reach equilibrium at the $O(1)$ orders in the long-wave approximation. Therefore, the influence of Bi, which modulates the adsorption/desorption flux, vanishes. It should be noted that Romanò *et al.* (2022) conducted an investigation into the nonlinear instability of the quiescent film. It indicated that R_b, Bi and Pe_b have little impact on the flow instability. This does not conflict with the results obtained in this study since parameter values are distinctively different.

4.3. *The film under an axial body force*

In this section, we proceed to consider the scenario of a film driven by an axial body force, e.g. gravity. Figure 9(*a*) depicts the growth rates versus wavenumber k with various R_b. When $R_b = 1000$, the curve of growth rate is close to that of the insoluble problem. As R_b decreases, the growth rates are reduced and the film tends to be linearly stable

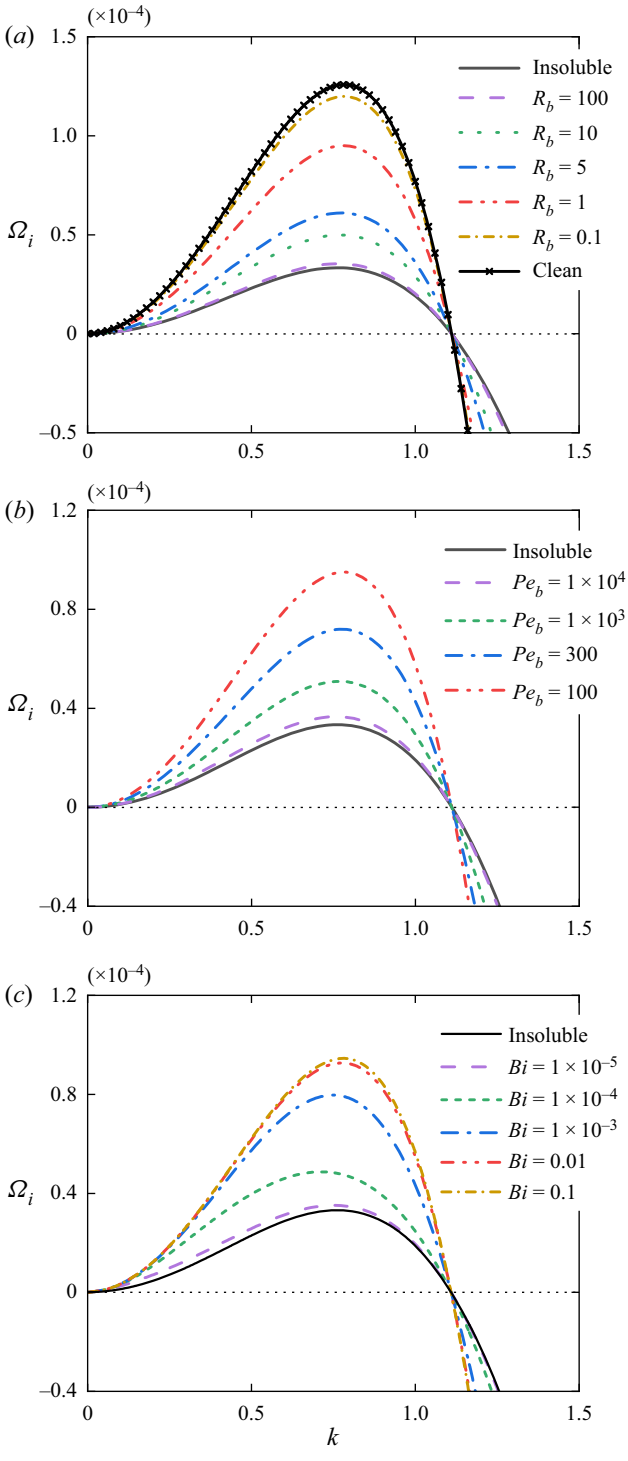

Figure 8. The dominant growth rate versus wavenumber k of a quiescent film under the influence of (a) solubility R_b, (b) bulk diffusivity Pe_b and (c) sorption kinetics Bi. In (a) $Bi = 0.1$ and $Pe_b = 100$ are adopted, in (b) $R_b = 1$ and $Bi = 0.1$ are adopted and in (c) $R_b = 1$ and $Pe_b = 100$ are adopted. The other parameters remain the same as in figure 2.

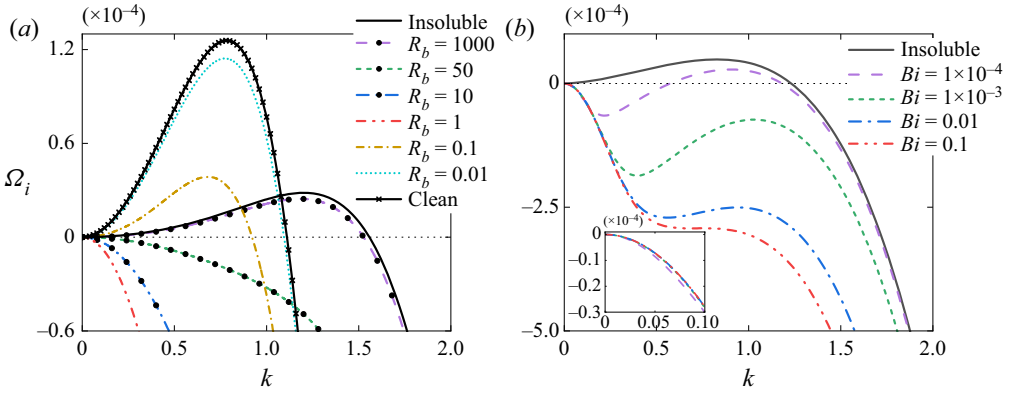

Figure 9. The dominant growth rate versus wavenumber k of a film driven by an axial body force under the influence of R_b and Bi. The results are obtained with $Bo = 1$ and $\tau = 0$. (a) Comparison of the growth rates of various R_b with $Ma = 0.02$, $Bi = 0.1$ and $Pe_b = 100$. (b) Comparison of the growth rates of various Bi with $Ma = 0.2$, $R_b = 1$ and $Pe_b = 100$. Other parameters take the same values as in figure 2.

eventually, as shown in the curves with $R_b = 50$ and 10. By continuously tracing the growth rates back to $k \ll 1$ (defined as the trace-back method in the following), the above curves are found to stem from the surfactant mode according to the long-wave approximation analysis. Thus, the modes corresponding to the above growth rate curves can be referred to as the surfactant modes. As illustrated in figure 9(a), it can be concluded that solubility plays a stabilizing role in the surfactant mode. This is in line with the prediction made by the long-wave approximation analysis. However, when R_b is decreased to $R_b^{(s)} = 3.138$, the most dangerous mode shifts from the surfactant mode to the interface mode, as depicted in figure 3. As R_b is further decreased, e.g. $R_b = 1.0, 0.1, 0.01$, the growth rates tend to increase, and the film flow is destabilized eventually. Particularly, at $R_b = 0.01$, the surfactant is highly soluble. The performance of the liquid film is similar to that of a clean interface with suppressed surface tension due to the presence of surface surfactant. Similar to figure 8(a), the growth rates are a little lower than those of the clean interface. Moreover, as illustrated in figure 9(a), it can be concluded that the film is linearly stabilized in the presence of soluble surfactant with intermediate solubility. A stability window can be observed ranging from $R_b = 0.165$ to $R_b = 113.579$ for the present setting of parameters. This is different from the situation with insoluble surfactant (Jain *et al.* 2022), where the surfactant mode is always unstable. Figure 9(b) shows the effect of sorption kinetics Bi on the dominant growth rates. Via the trace-back method, it is found that the instability of the film is dominated by the surfactant mode. In this regard, the main trigger for the instability is the accumulation/depletion of the surfactant at the interface. The results show that Bi strengthens the instability for the perturbations with long wavelength but attenuates the instability for the perturbations with finite wavelength. As $k \ll 1$ and Bi is increased from $Bi = 1 \times 10^{-4}$ to $Bi = 0.1$, the growth rates of the film increase as predicted by the long-wave approximation. However, for the perturbations with finite wavelength, the situation is reversed. The growth rates of the perturbation wave are decreased with increasing Bi. This is attributed to the fact that surfactant with larger sorption kinetics Bi can dissolve in the bulk more easily and improve the uniformity of the surface surfactant at the interface. Therefore, increasing Bi makes the perturbation wave more stable. Notably, these characteristics of Bi can stimulate an unstable region bounded away from the origin with $k = 0$, as shown by the curve for $Bi = 1 \times 10^{-4}$, which has been referred to as the mid-wave instability by Halpern & Frenkel (2003).

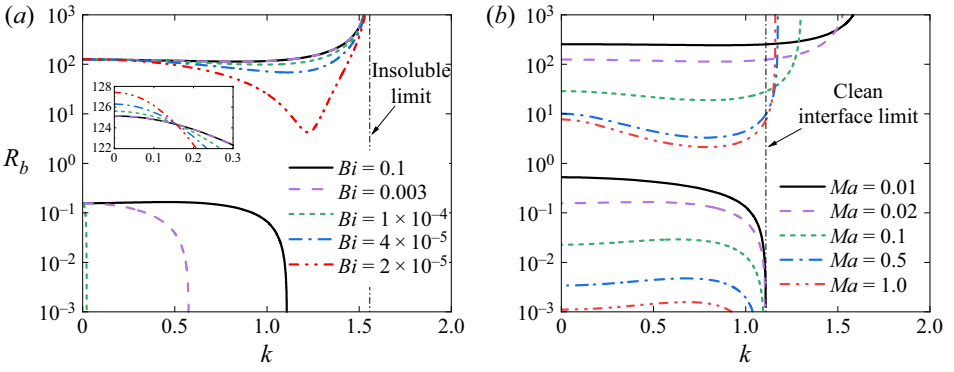

Figure 10. Neutral curves of a film driven by an axial body force with various (*a*) sorption kinetics Bi and (*b*) Marangoni numbers Ma. The results are obtained with $Bo = 1$ and $\tau = 0$. The parameters take $Ma = 0.02$ and $Pe_b = 100$ in (*a*) and $Bi = 0.1$ and $Pe_b = 100$ in (*b*). The other parameters remain the same as in figure 2.

Figure 10(*a*) shows the neutral curves of film linear instability on the k versus R_b plane with various Bi. For $Bi = 0.1$, there are two branches, which divide the neutral plane into three regions. The upper one corresponds to an unstable region for large R_b, which is caused by the surfactant mode. The lower one is also an unstable region, triggered by the interface mode instead. Between these two unstable regions, a stable region can be identified, which corresponds to the aforementioned stability window of R_b. As Bi is decreased, e.g. $Bi = 0.003$, 1×10^{-4}, the upper unstable region expands, whereas the lower unstable region shrinks. Particularly, when $Bi = 1 \times 10^{-4}$, the lower region almost disappears. This indicates that the instability of the interface mode can be suppressed with decreasing Bi. As Bi is further decreased to 4×10^{-5} and 2×10^{-5}, the upper unstable region continues to expand downward. In the limit of $Bi \to 0$, the neutral curves of the region degenerate into a vertical line with $k = 1.558$, which equals to the cut-off wavenumber of the problem with insoluble surfactant, as shown in figure 9(*a*). Figure 10(*b*) demonstrates the neutral curves on the k versus R_b plane for various Ma. When $Ma \ll 1$, the situation approximates to the case with clean interface and the curve degenerates into a vertical line with $k = 1/a$. For $Ma = 0.01$, similar to figure 10(*a*), there are two unstable regions, which arise from the surfactant mode and the interface mode, respectively. As Ma is increased from 0.02 to 1.0, the upper unstable region, which corresponds to the surfactant mode, expands when the maximal wavenumber of the unstable perturbation decreases. This indicates that the Marangoni effect can destabilize the surfactant mode with long wavelength while stabilize the surfactant mode with finite wavelength. However, for the lower unstable region, which corresponds to the interface mode, it shrinks with increasing Ma. In other words, the linear instability of the interface mode is suppressed due to the Marangoni effect. Similar results have been reported by Jain *et al.* (2022) in a problem with insoluble surfactant. It should be noted that the stable region, which is located between the upper and lower unstable regions, exists only under the situation with intermediate Ma. As $Ma \gg 1$, the interface becomes rigid and the neutral curves degenerate into $k = 1/a$ again.

Figure 11 illustrates the effect of bulk diffusivity Pe_b on the growth rates of the perturbations. It suggests that the bulk diffusivity of the surfactant plays a non-monotonic role in the linear instability of the film. When Pe_b is small, e.g. $Pe_b = 100$, the film is linearly stable. This is attributed to the stronger diffusivity of the bulk surfactant as Pe_b decreases. It tends to enhance the uniformity of the bulk surfactant distribution. Due to the

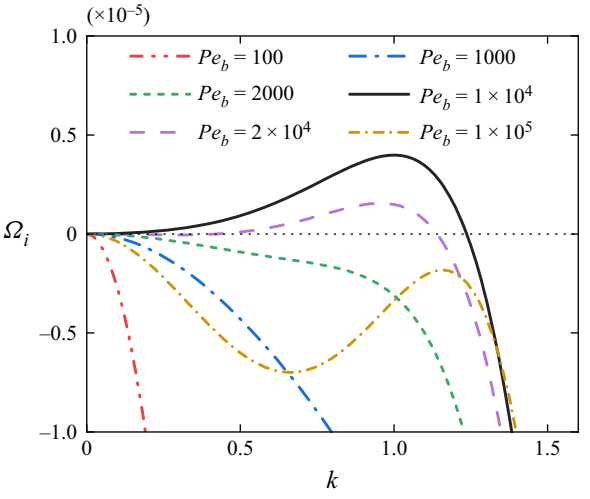

Figure 11. The dominant growth rate versus wavenumber k of a film driven by an axial body force under the influence of bulk diffusivity Pe_b. The parameters used here are $Bo = 1$, $\tau = 0$, $R_b = 10$ and $Bi = 0.1$. Other parameters take the same values as in figure 2.

Pe_b	100	1000	2000	1×10^4	2×10^4	1×10^5
$\arg(\hat{J}_b/\hat{\Gamma})$	132.0034°	95.2908°	92.8151°	91.4760°	92.1203°	99.0626°

Table 2. The phase shift between the perturbed adsorption/desorption flux $\hat{J}_b$ and the perturbed surface concentration $\hat{\Gamma}$ for various Pe_b at $k = 0.15$. Other parameters remain the same as in figure 11.

presence of the adsorption/desorption process, the concentration distribution of surface surfactant can also be improved, which acts to make the film stable. As Pe_b is increased from 100 to 1×10^4, the diffusivity of the bulk surfactant is weakened, and the film tends to become unstable. However, as Pe_b is further increased, e.g. $Pe_b = 2 \times 10^4$, 1×10^5, the growth rates of the perturbations decrease and the film finally becomes linearly stable again. Physically, this is caused by the sweeping effect of the base flow on the phase shift between $\hat{J}_b$ and $\hat{\Gamma}$. As listed in table 2, the value of phase shift is greater than 90°, and it increases as Pe_b is further increased. This indicates that there is an adsorption/desorption flux at the trough/crest of the $\hat{\Gamma}$ perturbation wave, which acts to improve the concentration distribution of the surface surfactant and make the film become stable.

4.4. *The film under an interfacial shearing force*

In this section, the linear instability of film flow driven by an interfacial shearing force is considered. Figure 12(*a*) demonstrates the growth rate versus wavenumber k for various solubility R_b. Similar to the results presented in figure 9(*a*), the growth rate curve is close to that of the insoluble case when R_b is large, e.g. $R_b = 10.0$. As R_b is decreased from 10 to 3, the instability of the film flow is dominated by the interface mode according to the trace-back method, and the growth rates of long-wave perturbations ($k \ll 1$) are augmented. This is in line with the long-wave results in figure 6. However, the situation is reversed as wavenumber k becomes larger. The growth rates for the perturbations

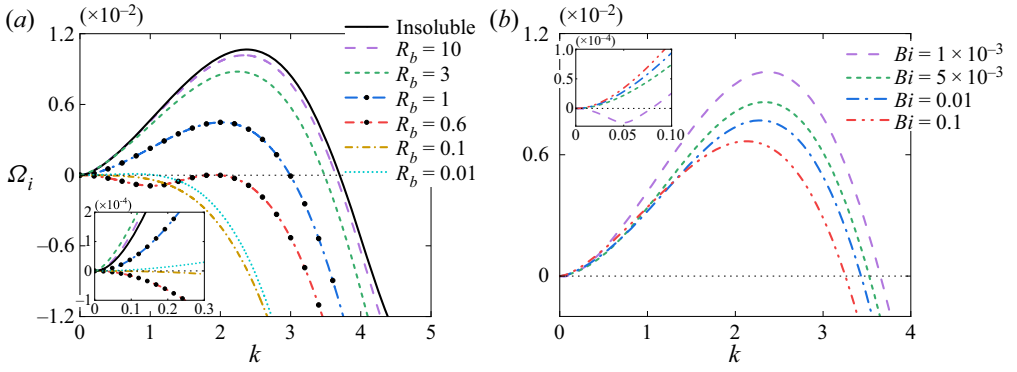

Figure 12. The dominant growth rate versus wavenumber k of a shear-driven film under the influence of R_b and Bi. The results are obtained at $Bo = 0$ and $\tau = 1$. (a) Comparison of the growth rates of different R_b with $Bi = 0.1$ and $Pe_b = 100$. (b) Comparison of the growth rates of different Bi with $R_b = 1.5$ and $Pe_b = 100$. Other parameters take the same values as in figure 2.

with finite wavelength decrease along R_b and so do the cut-off wavenumbers. When R_b becomes small enough, e.g. $R_b^{(c)} = 2.389$ for current parameter setting, the film instability is dominated by the surfactant mode instead of the interface mode. As R_b is decreased to 1.0 and 0.6, the results indicate that both growth rates and the cut-off wavenumbers are reduced, and the film even becomes stable. However, similar to film flow driven by an axial body force, as R_b is further decreased below 0.519, the surfactant mode is weakened by solubility and the interface mode becomes dominant again. As a result, the growth rates of the film increase and the film eventually becomes unstable again with an increase of solubility, as the curves with $R_b = 0.1$ and 0.01. Figure 12(b) presents the influence of sorption kinetics Bi on the linear instability of film flow. According to the trace-back method, we know that the film instability is dominated by the surfactant mode. It can be seen that the growth rates are increased with increasing Bi as $k \ll 1$. This indicates that Bi acts to destabilize the film with long-wave perturbations, as mentioned in the previous section. However, for the perturbation with finite wavenumber k, Bi tends to stabilize the film instead. This is similar to the role of Bi in a film driven by an axial body force.

In figure 13(a), the neutral instability curves on the k versus R_b plane with various Bi are presented. For $Bi = 0.1$, similar to film flow driven by an axial body force, there are two neutral branches and the plane is divided into three regions. However, unlike those presented in the previous section, the upper unstable region is attributed to both the surfactant mode and the interface mode. The lower unstable region still arises from the interface mode, and the stable region is located in the middle. As Bi is decreased from 0.04 to 0.03, it is observed that the upper unstable regions have changed. This suggests that for the film with slightly soluble surfactant ($R_b > 1.0$), the perturbations with long wavelength ($k \ll 1$) are suppressed with decreasing Bi. The opposite holds for the perturbations with finite wavelength (e.g. $k \approx 2.0$). However, as Bi decreases, the lower unstable region tends to expand continuously. When Bi becomes small enough, e.g. $Bi = 0.02$ and 0.01, the upper and lower unstable regions contact. The stable region in the middle is pinched off and degenerates into an island clinging to the R_b axis. This stable island shrinks as Bi decreases further. In the limit of the insoluble case with negligible sorption kinetics, i.e. $Bi \to 0$, the island vanishes and the unstable region takes up an area between $k = 0$ and $k = 3.698$, which is the cut-off wavenumber of the corresponding problem with insoluble surfactant. Figure 13(b) shows the effect of Marangoni number Ma

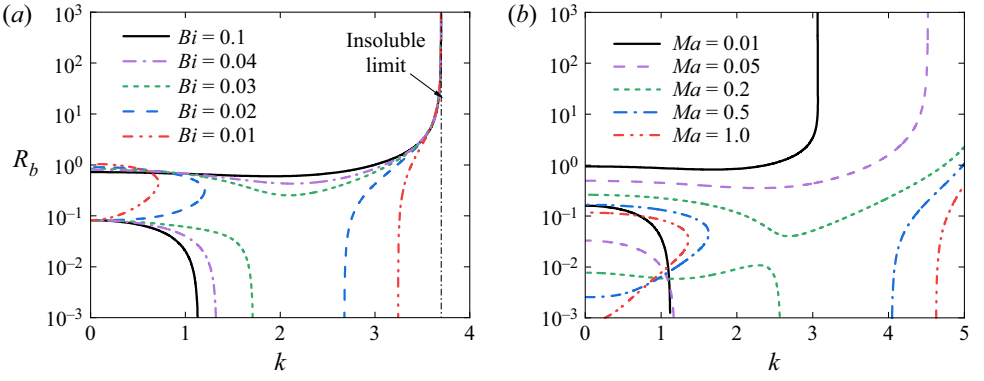

Figure 13. Neutral curves of a shear-driven film with various (*a*) sorption kinetics Bi and (*b*) Marangoni numbers Ma. The results are obtained with $Bo = 0$ and $\tau = 1$. The parameters take $Ma = 0.02$ and $Pe_b = 100$ in (*a*) and $Bi = 0.1$ and $Pe_b = 100$ in (*b*). The other parameters remain the same as in figure 2.

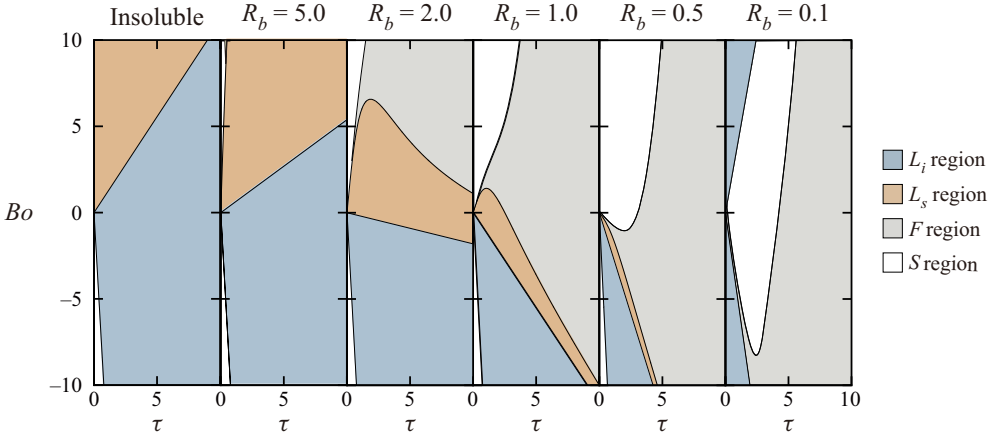

Figure 14. Unstable regions on the (τ, Bo) plane for various solubilities R_b. The parameters adopted here are $a = 0.9$, $Ma = 0.02$, $\bar{\Gamma} = 0.4$, $Bi = 0.1$, $Pe_b = 100$ and $Pe_s = 1 \times 10^6$. The sign of Bo or τ is positive, when the direction of the axial body force or the interfacial shearing force is downward. In the first panel for insoluble surfactant, when $\tau = 0$, the film is linearly unstable caused by the surfactant mode. This is consistent with the results presented in figure 3 based on long-wave approximation. Therefore, there is a neutral curve immediately adjacent to the axis with Bo less than zero, which distinguishes the unstable region caused by the surfactant mode, i.e. L_s region, from the stable region.

on the neutral instability. For $Ma = 0.01$, similar to figure 13(*a*), two unstable regions can be identified. As Ma is increased from 0.05 to 0.2, the upper unstable regions are expanded. This suggests that the Marangoni effect tends to destabilize the film with slightly soluble surfactant ($R_b > 1.0$). However, for the lower unstable region, it can be seen that the Marangoni effect acts to stir the instability of perturbations with finite wavelength. As Ma is increased further to 0.5 and 1.0, similar to figure 13(*a*), the upper and lower unstable regions contact. The stable region in the middle is pinched off, which leads to the appearance of a stable island as well. The island shifts downwards with increasing Ma.

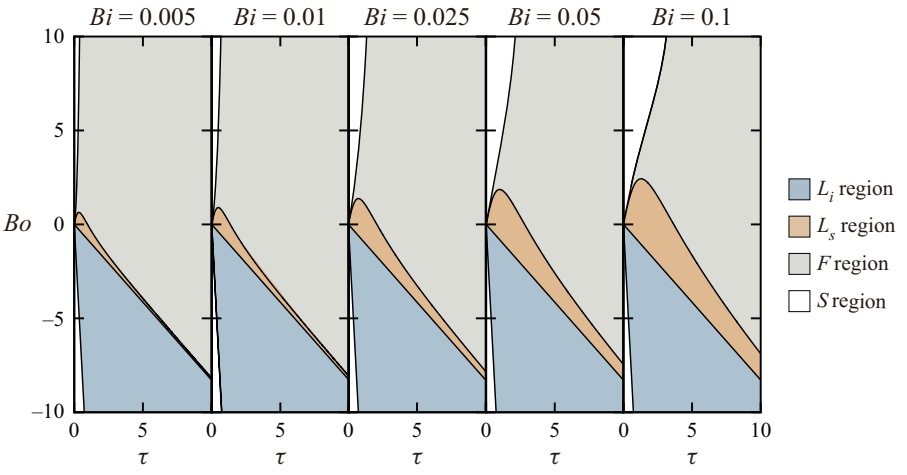

Figure 15. Unstable regions on the (τ, Bo) plane for various sorption kinetics Bi. The parameters adopted here are $a = 0.9$, $Ma = 0.02$, $\bar{\Gamma} = 0.4$, $R_b = 1.2$, $Pe_b = 100$ and $Pe_s = 1 \times 10^6$.

4.5. *Interaction between soluble surfactant and base flow*

In this section, film flow subjected to a combination of the axial body force and the interfacial shearing force is considered. Wei (2007) has demonstrated that a planar falling film with insoluble surfactant can be stabilized when the axial body force and the interfacial shearing force are in the opposite directions. For soluble surfactant, the situation can be more intricate, since the distribution of the surface surfactant will be influenced by the surfactant transport in the bulk.

Figure 14 depicts the neutral curves on the τ versus Bo plane with various R_b. The plane is divided into four regions, which are long-wave unstable region attributed to the interface mode (denoted as L_i), long-wave unstable region attributed to the surfactant mode (denoted as L_s), finite-wave unstable region (denoted as F) and linearly stable region (denoted as S). For the film contaminated with insoluble surfactant, it is susceptible to long-wave instability. A linearly stable S region can be detected, where film is subjected to a strong axial body force and a weak shearing force in opposite directions. When the soluble surfactant is considered, the unstable regions dominated by long-wave instability (L_i and L_s regions) tend to shrink with decreasing R_b. Further, new F region and S region emerge simultaneously. The new S region is located in the upper quadrant and enlarges with decreasing R_b. This suggests that the surfactant solubility can stabilize a film subjected to an axial body force and a shearing force in the same direction. This is totally different from that of the problem with insoluble surfactant. In the situation where $R_b = 0.1$, the L_s region nearly disappears, and the aforementioned S region, which used to be stable with insoluble surfactant, becomes unstable. As R_b is decreased further, solubility of the surfactant becomes very strong. It is conceivable that the concentration perturbation of surface surfactant would be mitigated by adsorption/desorption flux. The film would be destabilized due to the presence of the surface tension irrespective of the base flow. Therefore, it can be concluded that surfactant with intermediate solubility can achieve the best stabilizing effect for film flow.

Figure 15 demonstrates the effect of sorption kinetics Bi on the neutral curves. As Bi is increased, the L_i region tends to have little change. This is attributed to the fact that in the case of long-wave perturbation the instability of the interface mode is not affected by Bi as shown in (3.2). However, the L_s region expands with increasing Bi, which is

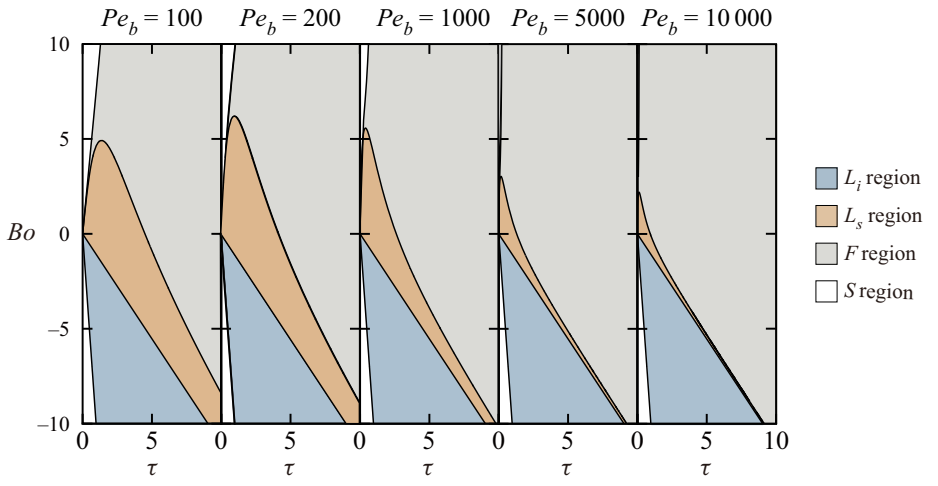

Figure 16. Unstable regions on the (τ, Bo) plane for various diffusivities Pe_b. The parameters adopted here are $a = 0.9$, $Ma = 0.05$, $\bar{\Gamma} = 0.4$, $R_b = 1.0$, $Bi = 0.1$ and $Pe_s = 1 \times 10^6$.

due to the role of $f_1^{(Bi)}$ in (A34). Similarly, the S region enlarges with an increase of Bi. Figure 16 demonstrates the influence of bulk diffusivity Pe_b on the neutral curves. Similar to figure 15, Pe_b has no impact on the L_i region because of the absence of Pe_b in c_1 of the long-wave interface mode. However, it plays a non-monotonic role in the L_s region. As shown in figure 16, when Pe_b is increased, the L_s region firstly enlarges, reaching its maximum area at intermediate Pe_b, and then shrinks. This indicates that surfactant with either small or large Pe_b contributes to stabilizing the perturbations with long wavelength. Moreover, in figure 16, the S region shrinks with increasing Pe_b. This may indicate that strong bulk diffusivity favours the linear stabilization of film flow.

5. Conclusion

In this study, we consider a film coating inside a rigid tube and laden with soluble surfactant. The flow is driven by an axial body force or an interfacial shearing force. The linear instability of the film with soluble surfactant subjected to various base flows is examined comprehensively. The problem is solved by long-wave approximation analysis and the spectral collocation method with Chebyshev polynomials. Two modes, which dominate the film instability, are identified and referred to as the interface mode and the surfactant mode, respectively. The effects of solubility R_b, sorption kinetics Bi and bulk diffusivity Pe_b on the linear instability of the film are discussed while ignoring the effect of inertia. For a quiescent film, they play a destabilizing role, which mitigate the perturbation of the surface surfactant and weaken the stabilizing effect of the Marangoni force.

When the film flow is driven by an axial body force (e.g. gravity), its instability exhibits more intricate features. It is found that the solubility R_b plays a destabilizing role in the interface mode. This is attributed to the adsorption/desorption flux of the surfactant, which reinforces the effect of surface surfactant transport induced by the base flow. It promotes the uniformity of the surface surfactant and thereby inhibits the stabilizing role of the Marangoni force. However, solubility R_b plays a stabilizing role on the surfactant mode instead. Consequently, the dual role of R_b may lead to a window with intermediate R_b, where the film can be linearly stabilized. The sorption kinetics Bi can destabilize the perturbations with long wavelength but stabilize the perturbations with finite wavelength,

potentially leading to mid-wave instability. For bulk diffusivity Pe_b, its influence on the flow instability is non-monotonic, which results in maximum growth rates at intermediate Pe_b. Notably, both weak and strong diffusivity of the bulk surfactant can suppress the flow instability. If the base flow is driven by an interfacial shearing force, in addition to the above conclusions, a critical solubility $R_b^{(c)}$ can be found. When $R_b > R_b^{(c)}$, the adsorption/desorption flux is found to hinder the effect of the surface surfactant transport attributed to the base flow, and exacerbate the non-uniformity of the surface surfactant. Consequently, solubility intensifies the destabilizing role of the Marangoni force. When $R_b < R_b^{(c)}$, the adsorption/desorption flux dominates the surface surfactant transport. Although the Marangoni force plays a stabilizing role under this circumstance, its influence is weakened as R_b decreases. For the surfactant mode, solubility is found to stabilize it on both sides of $R_b^{(c)}$. Furthermore, a more general problem involving both the axial body force and the interfacial shearing force is investigated. The neutral curves on the τ versus Bo plane indicate that surfactant with strong sorption kinetics and diffusivity and intermediate solubility tends to have the best stabilizing effect on film flow. Particularly, soluble surfactant can stabilize film flow driven by the axial body force and the shearing force in the same direction, which cannot be achieved by insoluble surfactant.

The current work sheds light on the mechanism of the linear instability of a film coating inside a tube. A valuable addition to this work would be the analysis of absolute/convective instability, as it offers valuable insights into the growth of disturbances observed and contributes significantly to practical application in experimental investigations. Moreover, this work may serve as a cornerstone for the systematic investigation of nonlinear dynamics which is considered in our following investigation, particularly in the context of the closure process for pulmonary airways. Additionally, the effects of inertia and non-axisymmetric perturbations on the instability are not clear yet. Further investigations into these problems are also of significance.

Acknowledgements. The authors would like to extend their heartfelt appreciation to the reviewers for their constructive comments and insightful suggestions. We would like to give special thanks to one of the reviewers, as she/he pointed out the potential limitations of the temporal instability analysis and provided guidance for our future work.

Funding. The authors acknowledge the support from NSFC grant no. 12072175.

Declaration of interests. The authors report no conflict of interest.

Author ORCIDs.
Sheng Li https://orcid.org/0000-0002-8828-3994;
Jie Peng https://orcid.org/0000-0001-9464-1658.

Appendix A. The long-wave approximation analysis process

A.1. *Geometrical parameters*

The geometrical parameters A_1–A_6, which are involved and correlated with the unperturbed radius of the liquid–air interface $r = a$, can be expressed as

$$\left.\begin{aligned} A_1 &= 1 - a^2 + 2a^2 \ln a, \quad A_2 = 1 - a^2 - 2a^2 \ln a, \\ A_3 &= 1 - 4a^2 + 3a^4 - 4a^4 \ln a, \quad A_4 = 1 - a^4 + 4a^4 \ln a, \\ A_5 &= 1 + 4a^2 - 5a^4 - 4a^4 \ln a, \quad A_6 = 1 - a^4 + 4a^2 \ln a. \end{aligned}\right\} \tag{A1}$$

In this study, A_1–A_6 are positive definite over $0 < a < 1$. Moreover, the combinations of these parameters involved in this investigation, i.e. $A_4 - 3A_6$ and $4a^2 - A_2$, are also positive when $a > 0.53$. It can be easily satisfied since we focus on the instability of a thin liquid film.

A.2. *Long-wave approximation expansion*

Substituting the expression (3.1) into (2.16)–(2.19*a–c*), the items with the same order of k are equated separately. For the leading order $O(1)$, the r-momentum equation and the normal force balance at the interface read

$$\mathrm{D}\hat{p}_0\,(r) = 0, \quad \hat{p}_0\,(a) = \frac{\bar{\gamma}}{a^2}\hat{\eta}_0 + \frac{Ma}{a\left(1-\bar{\Gamma}\right)}\hat{\Gamma}_0, \tag{A2a,b}$$

which yield a constant pressure across the film:

$$\hat{p}_0\,(r) = \frac{\bar{\gamma}}{a^2}\hat{\eta}_0 + \frac{Ma}{a\left(1-\bar{\Gamma}\right)}\hat{\Gamma}_0. \tag{A3}$$

Similarly, the z-momentum equation and corresponding boundary conditions are

$$\nabla^2\hat{\omega}_0 = 0, \tag{A4a}$$

$$\mathrm{D}\hat{\omega}_0\,(a) + \mathrm{D}^2\bar{\omega}\,(a)\,\hat{\eta}_0 = 0, \quad \hat{\omega}_0\,(1) = 0. \tag{A4b}$$

The expression of $\hat{\omega}_0(r)$ can be derived by integrating the above equations (A4). Then, we have

$$\hat{\omega}_0\,(r) = -a\mathrm{D}^2\bar{\omega}\,(a)\ln r. \tag{A5}$$

Substituting (A5) into the following continuity equation and no-slip condition at the tube wall ($r = 1$):

$$\mathrm{D}\hat{u}_0\,(r) + \frac{\hat{u}_0\,(r)}{r} + \mathrm{i}\hat{\omega}_0\,(r) = 0, \quad \hat{u}_0\,(1) = 0, \tag{A6a,b}$$

we can derive $\hat{u}_0(r)$ as

$$\hat{u}_0\,(r) = \mathrm{i}\mathrm{D}^2\bar{\omega}\,(a)\,\hat{\eta}_0\frac{1 - r^2 + 2r^2\ln r}{4r}. \tag{A7}$$

Substituting (A7) into the kinematic condition at the liquid–air interface $\hat{u}_0 = \mathrm{i}(\bar{\omega}(a) - c_0)\hat{\eta}_0$, we have

$$\left(c_0 - \bar{\omega}\,(a) + \frac{A_1}{4}\mathrm{D}^2\bar{\omega}\,(a)\right)\hat{\eta}_0 = 0. \tag{A8}$$

Similarly, for the leading order $O(1)$, the governing equation and boundary conditions of the bulk surfactant $\hat{C}_0$ can be derived as

$$\nabla^2\hat{C}_0 = 0, \quad \mathrm{D}\hat{C}_0\,(a) = \hat{J}_{b0}, \quad \mathrm{D}\hat{C}_0\,(1) = 0. \tag{A9a–c}$$

By integrating the above equation (A9*a–c*), we have

$$\hat{C}_0 = \frac{\hat{\Gamma}_0}{K_b(1-\bar{\Gamma})^2}. \tag{A10}$$

So far, it seems that the leading order cannot give adequate constraints for $\hat{\Gamma}_0$ and $\hat{C}_0$. Therefore, we turn to the first order, $O(k)$, equations. In the reference frame travelling with

c, the corresponding transport equation of the surface surfactant reads

$$SF_1^{(adv)} + SF_1^{(per)} = SF_1^{(dif)} + \hat{J}_{b1}, \tag{A11}$$

where

$$\left.\begin{aligned} SF_1^{(adv)} &= \mathrm{i}(\bar{\omega}(a) - c_0)\hat{\Gamma}_0, \quad SF_1^{(dif)} = 0, \\ SF_1^{(per)} &= \bar{\Gamma}\hat{u}_0(a)/a + \mathrm{i}\bar{\Gamma}(\hat{\omega}_0(a) + \mathrm{D}\bar{\omega}(a)\hat{\eta}_0), \\ \hat{J}_{b1} &= BiK_b(1-\bar{\Gamma})\hat{C}_1(a) - Bi(K_b\bar{C}+1)\hat{\Gamma}_1. \end{aligned}\right\} \tag{A12}$$

The governing equation and boundary conditions of the bulk surfactant $\hat{C}_1$ at the first order $O(k)$ can be derived as

$$\nabla^2\hat{C}_1(r) = \mathrm{i}Pe_b(\bar{\omega}(r) - c_0)\hat{C}_0, \tag{A13a}$$

$$\mathrm{D}\hat{C}_1(a) = Pe_b\beta\hat{J}_{b1}, \quad \mathrm{D}\hat{C}_1(1) = 0. \tag{A13b}$$

Here, by integrating (A13*a*) and combining with the boundary conditions (A13*b*), we get

$$\hat{J}_{b1} = -\mathrm{i}\frac{2\bar{q} - (1-a^2)c_0}{2a\beta}\hat{C}_0, \tag{A14}$$

where $\bar{q} = \int_a^1 r\bar{\omega}(r)\,\mathrm{d}r$. Substituting (A5), (A7) and (A14) into (A11), then we have

$$\left(\tau - \frac{A_2}{4a}\mathrm{D}^2\bar{\omega}(a)\right)\bar{\Gamma}\hat{\eta}_0 = (\bar{\omega} - c_0)\,\bar{\Gamma}_0 + \frac{2\bar{q} - (1-a^2)c_0}{2a\beta}\hat{C}_0. \tag{A15}$$

Thus, (A8), (A10) and (A15) are the basic equations for the long-wave approximation expansion. In the following, two modes, defined as the interface mode and the surfactant mode, are derived.

A.3. *The interface mode*

According to (A8), (A10) and (A15), the leading order $O(1)$ solutions of the interface mode, the wave celerity c_0, the perturbation of the surface surfactant $\hat{\Gamma}_0$ and the bulk surfactant $\hat{C}_0$ can be derived by setting $\hat{\eta}_0 = 1$ and $\hat{\eta}_1 = \hat{\eta}_2 = 0$:

$$c_0 = \bar{\omega}(a) - \frac{A_1}{4}\mathrm{D}^2\bar{\omega}(a), \tag{A16a}$$

$$\hat{\Gamma}_0 = \frac{(4a\tau - A_2\mathrm{D}^2\bar{\omega}(a))\bar{\Gamma}(1-\bar{\Gamma})^2}{aA_1\mathrm{D}^2\bar{\omega}(a)(1-\bar{\Gamma})^2 + 4(\bar{q} - (1-a^2)c_0/2)/R_b}, \tag{A16b}$$

$$\hat{C}_0(r) = \frac{\hat{\Gamma}_0}{K_b(1-\bar{\Gamma})^2}. \tag{A16c}$$

By definition, c_0 is a real number indicating marginal stability. Hence, the instability of the interface mode is to be determined by c_1. By integrating the governing equation and

boundary equations of $\hat{\omega}_1$,

$$\nabla^2\hat{\omega}_1\,(r) = \mathrm{i}\hat{p}_0, \tag{A17a}$$

$$\mathrm{D}\hat{\omega}_1\,(a) = \mathrm{i}\frac{Ma}{1-\bar{\Gamma}}\hat{\Gamma}_0 - \mathrm{D}^2\bar{\omega}\,(a)\,\hat{\eta}_1, \quad \hat{\omega}_1\,(1) = 0, \tag{A17b}$$

we have

$$\hat{\omega}_1\,(r) = -\mathrm{i}\hat{p}_0\frac{1-r^2+2a^2\ln r}{4} + \mathrm{i}a\frac{Ma\hat{\Gamma}_0}{1-\bar{\Gamma}}\ln r. \tag{A18}$$

Combining the continuity equation and no-slip condition at the wall,

$$\mathrm{D}\hat{u}_1\,(r) + \frac{\hat{u}_1\,(r)}{r} + \mathrm{i}\hat{\omega}_1\,(r) = 0, \quad \hat{u}_1\,(1) = 0, \tag{A19a,b}$$

the expression of u_1 is

$$\hat{u}_1(r) = \hat{p}_0\frac{(r^2-1)(r^2-1+2a^2)-4a^2r^2\ln r}{16r} + \frac{aMa\hat{\Gamma}_0}{1-\bar{\Gamma}}\frac{1-r^2+2r^2\ln r}{4r}. \tag{A20}$$

Substituting (A20) into the first-order $O(k)$ kinematic condition:

$$\hat{u}_1 = \mathrm{i}\,(\bar{\omega}\,(a) - c_0)\,\hat{\eta}_1 - \mathrm{i}c_1\hat{\eta}_0, \tag{A21}$$

c_1 of the interface mode can be expressed as

$$c_1 = \mathrm{i}\frac{A_3}{16a^3}\bar{\gamma} + \mathrm{i}\frac{A_4Ma}{16a^2(1-\bar{\Gamma})}\hat{\Gamma}_0. \tag{A22}$$

A.4. *The surfactant mode*

Similar to the derivation of the interface mode, the leading-order $O(1)$ solutions of the surfactant mode, i.e. the wave celerity c_0, the perturbation of the surface surfactant $\hat{\Gamma}_0$ and the bulk surfactant $\hat{C}_0$ can be derived according to (A8), (A10) and (A15) by setting $\hat{\Gamma}_0 = 1$ and $\hat{\Gamma}_1 = \hat{\Gamma}_2 = 0$:

$$c_0 = \frac{aR_b(1-\bar{\Gamma})^2\bar{\omega}(a) + \bar{q}}{aR_b(1-\bar{\Gamma})^2 + (1-a^2)/2}, \tag{A23a}$$

$$\hat{\eta}_0 = 0, \tag{A23b}$$

$$\hat{C}_0 = \frac{1}{K_b(1-\bar{\Gamma})^2}. \tag{A23c}$$

To determine the system instability, we proceed to render the first-order $O(k)$ solutions. According to (A17) and (A19a,b), we obtain

$$\hat{\omega}_1\,(r) = -\mathrm{i}\frac{Ma}{1-\bar{\Gamma}}\frac{1-r^2-2a^2\ln r}{4a} - a\mathrm{D}^2\bar{\omega}\,(a)\,\hat{\eta}_1\ln r, \tag{A24a}$$

$$\hat{u}_1(r) = \frac{Ma}{1-\bar{\Gamma}}\frac{(r^2-1)(r^2-1-2a^2)+4a^2r^2\ln r}{16ar} + \mathrm{i}a\mathrm{D}^2\bar{\omega}\,(a)\,\hat{\eta}_1\frac{1-r^2+2r^2\ln r}{4r}. \tag{A24b}$$

Here, $\hat{\eta}_1$ is determined by the combination of the first-order $O(k)$ kinematic conditions (A21), (A24*a*) and (A24*b*):

$$\hat{\eta}_1 = \mathrm{i}\frac{Ma}{1-\bar{\Gamma}}\frac{A_4}{4a^2\left(4c_0 + A_1\mathrm{D}^2\bar{\omega}\,(a) - 4\bar{\omega}\,(a)\right)}. \tag{A25}$$

For the perturbation of the bulk surfactant $\hat{C}_1(r)$, it is derived via (A13*a*) and (A13*b*) as

$$\hat{C}_1\,(r) = \frac{\mathrm{i}\,(\bar{\omega} - c_0)}{BiK_b\left(1-\bar{\Gamma}\right)} + \frac{\mathrm{i}\hat{C}_0}{64}Pe_bK\,(r)\,, \tag{A26}$$

where

$$\begin{aligned} K\,(r) = {} & 16\left(a^2 - r^2 + 2\ln r/a\right)c_0 + 16a\left[r^2 - a^2 - \left(1+r^2\right)\ln r + \left(1+a^2\right)\ln a\right]\tau \\ & + \left[\left(a^2-r^2\right)\left(r^2+9a^2-4\right) + 8a^2\left(r^2\ln r - a^2\ln a\right) + 4\left(2a^2-1\right)\ln r/a\right]Bo. \end{aligned} \tag{A27}$$

To obtain c_1, we turn to the advection–diffusion equation of the perturbed surface surfactant in the second order $O(k^2)$:

$$SF_2^{(adv)} + SF_2^{(per)} = SF_2^{(dif)} + \hat{J}_{b2}, \tag{A28}$$

with

$$\left.\begin{aligned} SF_2^{(adv)} &= -\mathrm{i}c_1\hat{\Gamma}_0, \quad SF_2^{(dif)} = -\hat{\Gamma}_0/Pe_s, \\ SF_2^{(per)} &= \bar{\Gamma}\hat{u}_1\,(a)/a + \mathrm{i}\bar{\Gamma}\left(\hat{\omega}_1(a) + \mathrm{D}\bar{\omega}(a)\hat{\eta}_1\right), \\ \hat{J}_{b2} &= BiK_b\left(1-\bar{\Gamma}\right)\hat{C}_2\,(a) - Bi\left(K_b\bar{C}+1\right)\hat{\Gamma}_2. \end{aligned}\right\} \tag{A29}$$

Here, $SF_2^{(adv)}$, $SF_2^{(per)}$, $SF_2^{(dif)}$ and $\hat{J}_{b2}$ are the four pathways for the transport of the surface surfactant in the second order $O(k^2)$ based on the reference frame where the perturbation wave is stationary. The governing equation and boundary conditions for the bulk surfactant $\hat{C}_2$ are

$$\nabla^2\hat{C}_2 = \mathrm{i}Pe_b\,(\bar{\omega} - c_0)\,\hat{C}_1 + \hat{C}_0 - \mathrm{i}Pe_b\hat{C}_0c_1, \tag{A30a}$$

$$\mathrm{D}\hat{C}_2\,(a) = Pe_b\beta_b\hat{J}_{b2}, \quad \mathrm{D}\hat{C}_2\,(1) = 0. \tag{A30b}$$

Integrating (A30*a*) with the constant determined by the boundary conditions (A30*b*), we have

$$\hat{J}_{b2} = \mathrm{i}\frac{1-a^2}{2aR_b\left(1-\bar{\Gamma}\right)^2}c_1 + f_1^{(Pe_b)} + f_1. \tag{A31}$$

Here,

$$f_1^{(Pe_b)} = -\frac{1-a^2}{2aPe_bR_b\left(1-\bar{\Gamma}\right)^2}, \tag{A32}$$

$$\begin{aligned} f_1 &= -\frac{\mathrm{i}}{a}\int_a^1 r\left(\bar{\omega}(r)-c_0\right)\hat{C}_1\,\mathrm{d}r \\ &= \underbrace{-\frac{\left((1-a^2)\bar{\omega}(a)-2\bar{q}\right)^2\left(1-\bar{\Gamma}\right)}{Bi\left(1-a^2+2aR_b\left(1-\bar{\Gamma}\right)^2\right)^2}}_{f_1^{(Bi)}} + \underbrace{\frac{Pe_bS}{64aR_b\left(1-\bar{\Gamma}\right)^2}}_{f_1^{(S)}} \end{aligned} \tag{A33}$$

and $S=\int_a^1 r(\bar{\omega}(r)-c_0)K(r)\,\mathrm{d}r$. Substituting (A24*a*), (A24*b*) and (A31) into (A28), c_1 of the surfactant mode can be expressed as

$$c_1 = \mathrm{i}\left(1+\frac{1-a^2}{2aR_b\left(1-\bar{\Gamma}\right)^2}\right)^{-1}\left(-\frac{1}{Pe_s}+f_1^{(Pe_b)}+f_1^{(Bi)}+f_1^{(S)}-SF_2^{(per)}\right). \tag{A34}$$

Here, $SF_2^{(per)}$, which indicates the second-order $\mathrm{O}(k^2)$ advective transport of the surface surfactant by the perturbed flow, can be expressed as

$$SF_2^{(per)} = \mathrm{i}\bar{\Gamma}\left(\frac{A_2\mathrm{D}^2\bar{\omega}(a)}{4a}-\tau\right)\hat{\eta}_1+\frac{A_5Ma\bar{\Gamma}}{16a^3\left(1-\bar{\Gamma}\right)}. \tag{A35}$$

A.5. *The quiescent film*

When the film is assumed to be quiescent, i.e. $Bo=0$ and $\tau=0$, we have $\bar{\omega}=\mathrm{D}^2\bar{\omega}=0$. According to (A8), by setting $\hat{\eta}_0=1$ and $\hat{\eta}_1=\hat{\eta}_2=0$, we have

$$c_0 = 0. \tag{A36}$$

Clearly c_0 is real, and the instability of the system is to be determined by c_1 as follows:

$$c_1 = \mathrm{i}\frac{A_3}{16a^3}\bar{\gamma}+\mathrm{i}\frac{A_4Ma}{16a^2(1-\bar{\Gamma})}\hat{\Gamma}_0. \tag{A37}$$

Since we consider the quiescent film, (A15) is fulfilled naturally. Therefore, $\hat{\Gamma}_0$ has to be determined by the second-order $O(k^2)$ equations of the surfactant. Combining (A28) and (A30), we have

$$\begin{aligned} &\mathrm{i}\left(1+\frac{1-a^2}{2aR_b\left(1-\bar{\Gamma}\right)^2}\right)\hat{\Gamma}_0c_1 \\ &\quad = \frac{A_4\bar{\gamma}\bar{\Gamma}}{16a^4}+\left(\frac{1}{Pe_s}+\frac{1-a^2}{2aPe_bR_b\left(1-\bar{\Gamma}\right)^2}+\frac{A_5Ma\bar{\Gamma}}{16\left(1-\bar{\Gamma}\right)a^3}\right)\hat{\Gamma}_0. \end{aligned} \tag{A38}$$

Solving (A37) and (A38) yields

$$\hat{\Gamma}_0 = \frac{-d_2\pm\sqrt{d_2^2-4d_1d_3}}{2d_1}, \tag{A39}$$

where parameters d_1, d_2 and d_3 are positive with the following expressions:

$$\left.\begin{aligned} d_1 &= \frac{A_4 Ma}{1-\bar{\Gamma}}\frac{\left(1-a^2\right)/R_b + 2a\left(1-\bar{\Gamma}\right)^2}{32a^3\left(1-\bar{\Gamma}\right)^2}, \\ d_2 &= \frac{1}{Pe_s} + \frac{1-a^2}{2aPe_bR_b\left(1-\bar{\Gamma}\right)^2} + \frac{A_5 Ma\bar{\Gamma}}{16a^3\left(1-\bar{\Gamma}\right)} + \frac{A_3\bar{\gamma}}{32a^4}\frac{\left(1-a^2\right)/R_b + 2a\left(1-\bar{\Gamma}\right)^2}{\left(1-\bar{\Gamma}\right)^2}, \\ d_3 &= \frac{A_4\bar{\gamma}\bar{\Gamma}}{16a^4}. \end{aligned}\right\} \tag{A40}$$

If the right-hand side of (A39) takes the '+' sign, (A37) may degenerate to $\mathrm{i}A_3\bar{\gamma}/16a^3$ as $R_b \gg 1$ and $Ma \ll 1$. This corresponds to c_1 of the interface mode for clean interface. Therefore, it can be classified as the interface mode. If (A39) takes the '−' sign, it corresponds to the surfactant mode. The corresponding c_1 yields $-\mathrm{i}/Pe_s$ as $R_b \gg 1$ and $Ma \ll 1$. According to numerical verification, the discriminant of (A39) is always non-negative under the current setting of the problem. It denotes that $\hat{\Gamma}_0$ is in opposite phase with $\hat{\eta}_0$. Therefore, the interface mode is the most dangerous mode, which determines the instability of the quiescent film.

Appendix B. Solutions near the critical solubility

As mentioned in § 3.3, the failure of the long-wave approximation is attributed to the fact that the adsorption/desorption flux offsets the effect of the surface surfactant transported by the base flow at $R_b^{(c)}$. Thus, the surface surfactant transported by the perturbed flow makes the surfactant infinitely accumulate/deplete. According to (A16*b*) or (A25), the critical solubility $R_b^{(c)}$ can be derived by letting the denominators be zero, which reads

$$R_b^{(c)} = \frac{\left(1-a^2\right)\left(4\bar{\omega}\left(a\right) - A_1\mathrm{D}^2\bar{\omega}\left(a\right)\right) - 2\bar{q}}{2aA_1\mathrm{D}^2\bar{\omega}\left(a\right)\left(1-\bar{\Gamma}\right)^2}. \tag{B1}$$

To resolve this issue, Frenkel & Halpern (2002) and Kalogirou & Blyth (2019) suggested expanding the variables by $k^{1/2}$ near the critical solubility. That is,

$$\begin{aligned} &\left\{\hat{\eta}, c, \hat{u}\left(r\right), \hat{\omega}\left(r\right), \hat{p}\left(r\right), \hat{\Gamma}, \hat{C}\left(r\right)\right\} \\ &\quad= \left\{\hat{\eta}_0, c_0, \hat{u}_0\left(r\right), \hat{\omega}_0\left(r\right), \hat{p}_0\left(r\right), \hat{\Gamma}_0/\sqrt{k}, \hat{C}_0\left(r\right)/\sqrt{k}\right\} \\ &\qquad + k^{1/2}\left\{\hat{\eta}_1, c_1, \hat{u}_1\left(r\right), \hat{\omega}_1\left(r\right), \hat{p}_1\left(r\right), \hat{\Gamma}_1/\sqrt{k}, \hat{C}_1\left(r\right)/\sqrt{k}\right\} + O\left(k^{3/2}\right). \end{aligned} \tag{B2}$$

Substituting the above equation (B2) into the linearized governing equations and boundary conditions (2.16)–(2.19*a–c*), we can derive (c_0, c_1) as

$$c_0 = \bar{\omega}\left(a\right) - \frac{A_1 D^2\bar{\omega}\left(a\right)}{4}, \tag{B3a}$$

$$c_1 = \pm\frac{(1-\mathrm{i})}{8}\sqrt{\frac{A_4 Ma\bar{\Gamma}\left(1-\bar{\Gamma}\right)\left(4a\tau - A_2 D^2\bar{\omega}\left(a\right)\right)}{a^2\left(\left(1-a^2\right)/R_b + 2a\left(1-\bar{\Gamma}\right)^2\right)}}. \tag{B3b}$$

Thus, the instability of the film flow can be determined according to $\mathrm{Im}(c_1)$ as well.

References

ADVANPIX, T. 2022 Multiprecision computing toolbox. http://www.advanpix.com.

BLYTH, M.G. & BASSOM, A.P. 2013 Stability of surfactant-laden core-annular flow and rod-annular flow to non-axisymmetric modes. *J. Fluid Mech.* **716**, R13.

BLYTH, M.G., LUO, H. & POZRIKIDIS, C. 2006 Stability of axisymmetric core-annular flow in the presence of an insoluble surfactant. *J. Fluid Mech.* **548**, 207–235.

BLYTH, M.G. & POZRIKIDIS, C. 2004 Effect of surfactants on the stability of two-layer channel flow. *J. Fluid Mech.* **505**, 59–86.

BOOTY, M. & SIEGEL, M. 2010 A hybrid numerical method for interfacial fluid flow with soluble surfactant. *J. Comput. Phys.* **229** (10), 3864–3883.

BREVDO, L., LAURE, P., DIAS, F. & BRIDGES, T.J. 1999 Linear pulse structure and signalling in a film flow on an inclined plane. *J. Fluid Mech.* **396**, 37–71.

CAMASSA, R., OGROSKY, H.R. & OLANDER, J. 2014 Viscous film flow coating the interior of a vertical tube. Part 1. Gravity-driven flow. *J. Fluid Mech.* **745**, 682–715.

CAMASSA, R., OGROSKY, H.R. & OLANDER, J. 2017 Viscous film-flow coating the interior of a vertical tube. Part 2. Air-driven flow. *J. Fluid Mech.* **825**, 1056–1090.

CAMPANA, D.M. & SAITA, F.A. 2006 Numerical analysis of the Rayleigh instability in capillary tubes: the influence of surfactant solubility. *Phys. Fluids* **18** (2), 022104.

CRASTER, R., MATAR, O. & PAPAGEORGIOU, D. 2009 Breakup of surfactant-laden jets above the critical micelle concentration. *J. Fluid Mech.* **629**, 195–219.

D'ALESSIO, S., PASCAL, J., ELLABAN, E. & RUYER-QUIL, C. 2020 Marangoni instabilities associated with heated surfactant-laden falling films. *J. Fluid Mech.* **887**, A20.

DALKILIC, A.S. & WONGWISES, S. 2009 Intensive literature review of condensation inside smooth and enhanced tubes. *Intl J. Heat Mass Transfer* **52** (15–16), 3409–3426.

EDWARDS, D.A., BRENNER, H. & WASAN, D.T. Ed.1991 *Interfacial Transport Processes and Rheology*. Butterworth-Heinemann.

FRENKEL, A.L. & HALPERN, D. 2002 Stokes-flow instability due to interfacial surfactant. *Phys. Fluids* **14** (7), L45–L48.

GASTER, M. 1962 A note on the relation between temporally-increasing and spatially-increasing disturbances in hydrodynamic stability. *J. Fluid Mech.* **14** (2), 222–224.

GOREN, S.L. 1962 The instability of an annular thread of fluid. *J. Fluid Mech.* **12** (2), 309–319.

GROTBERG, J.B. 2001 Respiratory fluid mechanics and transport processes. *Annu. Rev. Biomed. Engng* **3** (1), 421–457.

HALPERN, D. & FRENKEL, A.L. 2003 Destabilization of a creeping flow by interfacial surfactant: linear theory extended to all wavenumbers. *J. Fluid Mech.* **485**, 191–220.

HALPERN, D. & GROTBERG, J.B. 1993 Surfactant effects on fluid-elastic instabilities of liquid-lined flexible tubes: a model of airway closure. *Trans. ASME J. Biomech. Engng* **115** (3), 271–277.

HAMMOND, P. 1983 Nonlinear adjustment of a thin annular film of viscous fluid surrounding a thread of another within a circular cylindrical pipe. *J. Fluid Mech.* **137**, 363–384.

HASEGAWA, E. & NAKAYA, C. 1970 Stability of a liquid layer down the surface of a vertical cylinder. *J. Phys. Soc. Japan* **29** (6), 1634–1639.

HU, H.H. & PATANKAR, N. 1995 Non-axisymmetric instability of core-annular flow. *J. Fluid Mech.* **290**, 213–224.

JAIN, N., SHARMA, G. & DAS, S. 2022 Instability of liquid film flow inside of a vertical tube in presence of an interfacial surfactant. *Phys. Rev.* E **106**, 055101.

JOSEPH, D.D., BAI, R., CHEN, K. & RENARDY, Y.Y. 1997 Core-annular flows. *Annu. Rev. Fluid Mech.* **29** (1), 65–90.

KALOGIROU, A. & BLYTH, M. 2019 The role of soluble surfactants in the linear stability of two-layer flow in a channel. *J. Fluid Mech.* **873**, 18–48.

KALOGIROU, A. & BLYTH, M. 2021 Instabilities at a sheared interface over a liquid laden with soluble surfactant. *J. Engng Maths* **129**, 3.

KALOGIROU, A. & BLYTH, M.G. 2020 Nonlinear dynamics of two-layer channel flow with soluble surfactant below or above the critical micelle concentration. *J. Fluid Mech.* **900**, A7.

KARAPETSAS, G. & BONTOZOGLOU, V. 2013 The primary instability of falling films in the presence of soluble surfactants. *J. Fluid Mech.* **729** (4), 123–150.

KARAPETSAS, G. & BONTOZOGLOU, V. 2014 The role of surfactants on the mechanism of the long-wave instability in liquid film flows. *J. Fluid Mech.* **741**, 139–155.

KRANTZ, W.B. & ZOLLARS, R.L. 1976 The linear hydrodynamic stability of film flow down a vertical cylinder. *AIChE J.* **22** (5), 930–934.

KWAK, S. & POZRIKIDIS, C. 2001 Effect of surfactants on the instability of a liquid thread or annular layer. Part I. Quiescent fluids. *Intl J. Multiphase Flow* **27** (1), 1–37.

MURADOGLU, M., ROMANÒ, F., FUJIOKA, H. & GROTBERG, J. 2019 Effects of surfactant on propagation and rupture of a liquid plug in a tube. *J. Fluid Mech.* **872**, 407–437.

OGROSKY, H.R. 2021 Linear stability and nonlinear dynamics in a long-wave model of film flows inside a tube in the presence of surfactant. *J. Fluid Mech.* **908**, A23.

OTIS, D. JR., JOHNSON, M., PEDLEY, T. & KAMM, R. 1993 Role of pulmonary surfactant in airway closure: a computational study. *J. Appl. Physiol.* **75** (3), 1323–1333.

PENG, J. & ZHU, K.-Q. 2010 Linear instability of two-fluid Taylor–Couette flow in the presence of surfactant. *J. Fluid Mech.* **651**, 357–385.

RAYLEIGH, LORD 1892 XVI. On the instability of a cylinder of viscous liquid under capillary force. *Lond. Edinb. Dubl. Phil. Mag. J. Sci.* **34** (207), 145–154.

ROMANÒ, F., MURADOGLU, M. & GROTBERG, J.B. 2022 Effect of surfactant in an airway closure model. *Phys. Rev. Fluids* **7**, 093103.

SAMANTA, A. 2014 Shear-imposed falling film. *J. Fluid Mech.* **753**, 131–149.

STONE, H.A. 1990 A simple derivation of the time-dependent convective-diffusion equation for surfactant transport along a deforming interface. *Phys. Fluids* A **2** (1), 111–112.

STONE, H.A., STROOCK, A.D. & AJDARI, A. 2004 Engineering flows in small devices: microfluidics toward a lab-on-a-chip. *Annu. Rev. Fluid Mech.* **36**, 381–411.

TREFETHEN, L.N. 2000 *Spectral Methods in MATLAB*. SIAM.

WEI, H.-H. 2005 Effect of surfactant on the long-wave instability of a shear-imposed liquid flow down an inclined plane. *Phys. Fluids* **17** (1), 012103.

WEI, H.-H. 2007 Role of base flows on surfactant-driven interfacial instabilities. *Phys. Rev.* E **75** (3), 036306.

WEI, H.-H. & RUMSCHITZKI, D.S. 2005 The effects of insoluble surfactants on the linear stability of a core-annular flow. *J. Fluid Mech.* **541**, 115–142.

WONG, H., RUMSCHITZKI, D. & MALDARELLI, C. 1996 On the surfactant mass balance at a deforming fluid interface. *Phys. Fluids* **8** (11), 3203–3204.

XU, J., LIU, J., ZHANG, Z. & WU, X. 2023 Spatial-temporal transformation for primary and secondary instabilities in weakly non-parallel shear flows. *J. Fluid Mech.* **959**, A21.

ZHOU, Z.-Q., PENG, J., ZHANG, Y.-J. & ZHUGE, W.-L. 2014 Instabilities of viscoelastic liquid film coating tube in the presence of surfactant. *J. Non-Newtonian Fluid Mech.* **204**, 94–103.